Keratin 15 promotes a progenitor cell state in basal keratinocytes of skin epidermis

Catherine J. Redmond[1], Sarah N. Steiner[1], Erez Cohen[1],
Craig N. Johnson[1], Nurhan Özlü[2] and Pierre A. Coulombe[1,3,4,#]

[1] Department of Cell & Developmental Biology, University of Michigan Medical School, Ann Arbor, MI
[2] Department of Molecular Biology and Genetics, Science Faculty, Koç University, Istanbul, Turkey
[3.] Department of Dermatology, University of Michigan Medical School, Ann Arbor, MI
[4] Rogel Cancer Center, University of Michigan, Ann Arbor, MI.

[#] Corresponding author. Address: Pierre A. Coulombe, Ph.D., Dept. of Cell & Developmental Biology, University of Michigan Medical School, 109 Zina Pitcher Place, Ann Arbor, MI 48109, USA. ; E-mail: coulombe@umich.edu ; Tel: 734-615-7509.

Short title: Keratin 15 promotes the progenitor epithelial state

Key words: skin, stratified epithelia, epidermis, keratinocyte, keratin, intermediate filament, homeostasis, progenitor, stem cell, differentiation, Hippo signaling, single cell biology, RNAseq.

SUMMARY

The type I intermediate filament proteins keratin 14 (K14) and keratin 15 (K15) are common to all complex epithelia. K14 is highly expressed by progenitor keratinocytes, in which it provides essential mechanical integrity and gates keratinocyte entry into differentiation by sequestering YAP1, a transcriptional effector of Hippo signaling, to the cytoplasm. K15 has long been used as a marker of hair bulge stem cells though its specific role in skin epithelia is unknown. Here we show that the lack of two biochemical determinants, a cysteine residue within the stutter motif of the central rod domain and a 14-3-3 binding site in the N-terminal head domain, renders K15 unable to effectively sequester YAP1 in the cytoplasm. We combine insight obtained from cell culture and transgenic mouse models with computational analyses of transcriptomics data and propose a model in which the K15:K14 ratio promotes a progenitor state and antagonizes differentiation in keratinocytes of the epidermis.

INTRODUCTION

Complex epithelia function as physical, chemical and immunological barriers in many organs and tissues across the body, including the skin, eye, oral mucosa, and reproductive tract. The barrier function of these epithelia is maintained throughout life by carefully balancing the growth, via proliferation, and loss, via differentiation, of keratinocytes, the predominant cell type within complex epithelia, through the process of epithelial homeostasis [1,2].

Keratinocytes can be characterized by their denominal, keratin intermediate filament (IF) proteins. Owing to their diversity (N=54 in humans), differentiation-dependent regulation, unique mechanical properties, and post-translational modifications, keratin IF proteins play important roles in specific aspects of keratinocyte biology in addition to maintenance of epithelial integrity [3-5]. The transcriptional and post-translational regulation of keratin genes and proteins, and their impact on the complex process of epithelial homeostasis, are under active investigation [6]. In order to sustain the long-term regeneration of complex epithelia, epithelial homeostasis requires stem-like progenitor keratinocytes that maintain mitotic competency over decades of life [1,2]. Here, we provide evidence for a mechanism that prevents the differentiation-related premature loss of progenitor keratinocytes through the regulation of the mechanosensitive transcriptional co-activator YAP1 by keratin IF proteins.

Common to all complex, stratified (e.g., epidermis) and pseudostratified epithelia (e.g., trachea) is the expression of the type I keratins 14 and 15 (K14, K15) and their type II co-polymerization partner K5 [3 4]. K5 and K14 mRNA and proteins are prominently co-expressed in all keratinocytes residing in the basal layer of stratified epithelia [5]. K5/K14 IFs comprise the majority of the mechanical resilience of these cells, protecting them again shear- and trauma-induced lysis [7,8]. In support of the latter, small, dominantly-acting missense variants affecting the polymerization and mechanical properties of either K5 or K14 are causative for epidermolysis bullosa simplex (EBS), a rare genetic skin disorder in which basal layer keratinocytes are fragile and shear or lyse in response to trauma [7]. In striking contrast, very little is known about K15, other that the intriguing attribute that it is correlated, cell-autonomously, with stemness in the skin [9,10] and other stratified epithelia [11].

Additional to its well-defined structural function, a novel role for K14 recently came to the fore through the characterization of mice carrying a *Krt14* C373A mutant allele [12]. *Krt14* C373A mutant mice were generated to study the physiological significance of a disulfide bond discovered in a crystal structure of the interacting 2B coiled-coil rod domains of human K5 and K14 [13]. This homotypic transdimer disulfide linkage was shown to involve cysteine (C) 367, located in the 2B domain of human K14 [13] (note: C367 in human K14 corresponds to C373 in

mouse K14). What sets this specific residue apart from other cysteines in human and mouse K14 is its location as the second residue of the so-called stutter motif, a four-residue disruption of the long-range heptad repeats that is nearly perfectly conserved across the entire superfamily of IF proteins [13]. Intriguingly, a cysteine residue occurs in the second position of the stutter in several type I keratins expressed in surface epithelia, including the differentiation-specific K9 and K10 [13] and the stress-induced K16 and K17 [12]. Further, a crystal structure of the interacting 2B domains of K10 and its type II partner K1 also uncovered a homotypic disulfide linkage mediated by the K10 stutter cysteine [14].

Follow-up live imaging studies of skin keratinocytes in primary culture revealed that the K14 stutter cysteine is required for the establishment of the perinuclear filament network [15], a trademark feature in early-stage differentiating keratinocytes of surface epithelia [13,16]. The *Krt14* knock-in mutant C373A mouse was thus generated to test the physiological role of C373-dependent perinuclear disulfide bonding. Loss of K14 C373 in these mutant mice caused a delay in the initiation of keratinocyte differentiation and aberrant terminal differentiation, ultimately resulting in a barrier defect [12]. Mutagenesis studies involving newborn skin keratinocytes in primary culture coupled with a proteomics screen for K14-interacting proteins revealed that, unlike its wildtype counterpart, the K14 C373A protein is unable to promote the cytoplasmic retention of YAP1, a terminal (co-transcriptional) effector of Hippo signaling [17], as epidermal keratinocytes are called upon to initiate differentiation *in vivo* or in culture [12]. Alongside YAP1 dysregulation, 14-3-3σ, a YAP1-interacting protein [18], occurs in an aggregated rather than the normal diffuse pattern in epidermal keratinocytes of *Krt14* C373A mice [12]. These findings guided the development of a model whereby the stutter cysteines in K14 and K10 are required for the cytoplasmic retention of YAP1, in a 14-3-3-dependent manner, thus mediating the initiation (via K14) and sustainment of differentiation (via K10) in epidermal keratinocytes.

Relative to K14, the K15 mRNA and protein are expressed in a subset of keratinocytes in the basal layer [19,20]. Studies that followed up on the discovery of K15's enrichment in the hair bulge [9] strengthened the correlation of K15 in epithelial stem cells of the skin [10]. K15 has since been described as a marker for progenitor cells in several epithelial-rich organs and its expression has been correlated to the development and severity of cancers in these tissues [10]. Despite the breadth of work relating K15 to stemness and cancer, a functional role has yet to be assigned to this type I keratin. In human and mice lacking K14 protein, K15 and K5 form fine ("wispy") filaments in basal keratinocytes that fail to compensate for the essential structural function of K14/K5 filaments [19,21-23]. Critically, unlike K14 or K10, K15 does not feature a cysteine at the second position of the stutter motif in its 2B domain.

Here, we combine biochemical, cell biological, histological, computational and physiological evidence to show that, through its spatially unique distribution and expression levels in epidermis, its lack of a stutter cysteine and a lesser ability to promote the cytoplasmic sequestration of YAP1, K15 functions as a negative regulator of keratinocyte differentiation and promotes the progenitor cellular state in skin epithelia.

RESULTS

K15 occurs in a spatially defined pool of progenitor keratinocytes in human epidermis

K14 is widely considered, and used, as a marker for "mitotically-competent progenitor keratinocytes" in the basal layer of stratified epithelia, including the epidermis. However, several studies have shown that the expression pattern of K14, at both the protein [24] and mRNA levels [25], is broader and includes early-stage terminally differentiating keratinocytes in the lower suprabasal compartment of epidermis [5]. Immunostaining for K14 in human thin (buttock) skin sections corroborates this (Fig. 1A). K15 displays a distinct immunostaining pattern, in that it is largely excluded from the suprabasal compartment and shows markedly brighter signal in basal keratinocytes located in bottom of rete ridges (Fig. 1A). Co-staining for K15 and K10 in thin epidermis shows a strict exclusion between the $K15^+$ basal and $K10^+$ suprabasal compartments (Fig. 1B,B'). These findings are consistent with and extend previous studies [19,20,26-29]. Analyses of newborn mouse skin keratinocytes in primary culture under calcium-free, growth-promoting conditions shows that bright K14 immunostaining occurs in all keratinocytes whereas K15 is only present in a subset of the cells (Fig. 1C; quantitation shown in Fig. 1C'). These observations, and others derived from mouse skin in situ (see below), establish that the differences in K14 and K15 expression patterns are largely conserved in human and mouse.

Single cell transcriptomics reveal attributes unique to KRT15-expressing keratinocytes

The availability of single cell (sc) RNA-seq datasets affords an opportunity to gain insight into the significance of keratin gene expression in human skin [5]. In healthy abdominal (thin) skin (Suppl. Fig. 1A), the majority of keratinocytes can be partitioned into two subsets that exhibit either a *KRT14*-high or *KRT10*-high signature, representing progenitor or differentiating status, respectively (Suppl. Fig. 1B,C; see [5]). A third, sizable group of keratinocytes exhibit a hybrid character with appreciable expression of both *KRT14* and *KRT10* (Suppl. Fig. 1D) [5]. By comparison, *KRT15* expression (Suppl. Fig. 1E) occurs only in a subset of *KRT14*-expressing keratinocytes (Fig. 2A). These *KRT15*-expressing cells show minimal overlap with *KRT10*-expressing cells (Fig. 2B). Directly relating the number of *KRT15* to *KRT14* reads across the

population of individual keratinocytes in human trunk skin (N=26,063 cells) [5], in the form of a scatter plot, further highlights that *KRT15*-expressing keratinocytes are a subset of *KRT14*-expressing ones (Fig. 2C). Additionally, we find that the number of *KRT15* reads per cell is, overall, significantly lower than that of *KRT14* in trunk skin keratinocytes (Fig. 2D). These findings are consistent with the immunostaining data reported in Fig. 1.

To probe deeper into the transcriptional signature that reflects the progenitor cellular state, we next performed a supervised analysis of the entire keratinocyte population of thin epidermis according to composite scores [5,30]: a “basal score” to identify cells with high transcriptional activity for genes relating to the extracellular matrix (and thus likely to reside in the basal compartment), a “differentiation score” to identify cells engaged into differentiation (e.g., cell-cell adhesion components), and “G2/M” and “S” scores to identify cells undergoing mitosis. These scores are formulated independently of any keratin gene (see Methods and [5]).

First, we sorted individual keratinocytes according to their expression of a given keratin gene as a function the basal score, with the latter binned into quartiles (percentiles 0-25, 26-50, 51-75 and 76-100). This analysis revealed that *KRT15* expression shows a clear bias towards keratinocytes with a high basal score, *KRT10* expression shows a clear bias towards keratinocytes with a lower basal score, while *KRT14* expression shows a mixed identity (Fig. 2E). Second, we rank-ordered the Seurat clusters (Suppl. Fig. 1A) according to the ratio of their “basal” and “differentiation” scores. This analysis revealed a clear sequence whereby *KRT15* occurs in cells with a clear basal identity, *KRT14* occurs across cells with either a basal or a differentiating identity, and *KRT10* expression is polarized to differentiating cells (Fig. 2F). Third, we related keratin expression to the G2/M composite score, which reflects engagement in mitosis. This analysis showed that even though they exhibit a high basal score, high *KRT15*-expressing keratinocytes show very low G2M scores, unlike high *KRT14*-expressing cells (Fig. 2G). The same conclusion is attained when relating *KRT15* and *KRT14* expression to a composite score for S Phase (Suppl. Fig. 1F,G). By contrast, the relationship between *KRT10* expression levels and the G2/M score is clearly bimodal (Suppl. Fig. 1H), consistent with the recent demonstration of a transitional population of epidermal keratinocytes that have initiated differentiation and yet are mitotically-active [5,31,32]. Interestingly, the Seurat cluster enriched for G2/M keratinocytes maps to cells that feature an intermediate basal-to-differentiation score in the distribution reported in Fig. 2F. This analysis also revealed that *KRT15* is distinct from *KRT14* in its transcriptional regulation relative to a type II keratin partner. As reported [5], transcription of *KRT14* and *KRT5* (R^2=0.79), and similarly of *KRT10* and *KRT1* (R^2=0.84), are tightly correlated over a broad range of expression levels (Fig. 2H). By contrast, *KRT15* shows a

markedly weaker correlation to *KRT5* (R^2=0.31; Fig. 2H) or any other type II keratin gene (data not shown). How the apparent imbalance in type I (*KRT14*, *KRT15*) and type II (*KRT5*) keratin transcripts is resolved at the protein level in progenitor keratinocytes of thin epidermis is an issue of interest but was not addressed as part of the current study.

On average, therefore, *KRT15* is highly expressed by cells with the strongest basal and weakest differentiated identity while *KRT10* is highly expressed by cells with the weakest basal and strongest differentiated identity. Further substantiating the distinct character of *KRT15*, the top 24 genes showing highest correlation to *KRT15* in human trunk skin (all cells) are highly enriched for components of hemidesmosomes and extracellular matrix (ECM) (Fig. 3A,B). In contrast, the top 24 genes most correlated to *KRT10* in human trunk skin (all cells) are highly enriched for desmosome components and proteins involved in terminal differentiation (Fig. 3A,C). These analyses confirm that *KRT15* and *KRT10* respectively define the progenitor vs. differentiating status while *KRT14* exhibits a broader distribution that spans both states in the epidermis.

Attributes of KRT15-expressing keratinocytes are also manifested in human foreskin and mouse back skin

Relative to trunk skin, *KRT15* is more prominently expressed in human foreskin (Suppl. Fig. 2A-D). Still, the basic attributes defining *KRT15* expression in human trunk (thin) skin (Fig. 2) apply to this tissue (Suppl. Fig. 2). Partitioning keratinocytes into quartiles according to the composite basal score (see Methods) highlights an enrichment for *KRT15* in keratinocytes within the quartiles showing the highest basal score and an enrichment for *KRT10* the quartiles showing the lowest basal score (Suppl. Fig. 2E). *KRT14*, on the other hand, manifests a hybrid character in this analysis (Suppl. Fig. 2E). A similar outcome is seen when organizing clusters according to the ratio of basal-to-differentiating scores (compare Suppl. Fig. 2F with Fig. 2F). Besides, an enrichment for G2-M^{high} keratinocytes in *KRT14*^{high} keratinocytes is also maintained while a fraction of *KRT15*^{high} keratinocytes show a high G2-M score in foreskin (Suppl. Fig. 2G). Further, relative to trunk skin, the correlation between *KRT5* and *KRT15* expression is stronger in foreskin (R^2=0.43 vs. R^2=0.31, respectively), while the *KRT5*-*KRT14* and *KRT1*-*KRT10* pairings still manifest an extraordinarily high correlation (R^2=0.73 vs. R^2=0.84, respectively; Suppl. Fig. 2 H,H'). While *KRT15* shows more prominent expression in foreskin, it retains its character as a transcript that is enriched in a subpopulation of progenitor keratinocytes that show a strong basal character (Suppl. Fig. 2).

Similar analyses performed in a single cell transcriptomics data set obtained from mouse back skin (see Methods) show that the attributes that define *KRT15* expression in human trunk skin and foreskin are largely maintained in mouse skin compartment (Suppl. Fig. 3A-H').

A candidate 14-3-3 binding site in the N-terminal head domain of K14 is missing in K15

We next sought to test the hypothesis that K15 and K14 fundamentally differ in their ability to sequester YAP1 to the cytoplasm, reflecting the presence or absence of the stutter cysteine along with a 14-3-3 binding motif (Fig. 4A). 14-3-3σ has been shown to play a role in the cytoplasmic sequestration of YAP1 at an early stage of keratinocyte differentiation in the interfollicular epidermis [33,34]. K14 physically associates with, and is spatially proximal to, 14-3-3σ in newborn mouse skin keratinocytes as shown by co-immunoprecipitation and PLA [12]. The relevant cis-acting determinant(s) on K14 are, however, unknown. 14-3-3 adaptor proteins typically bind their client proteins, including YAP1 [35], in a phosphorylation-dependent manner [36]. Several IF proteins, in addition to K14, can bind 14-3-3 adaptors. For human K17 [37], human K18 [38], Xenopus K19 [39] and human vimentin [40], mutagenesis studies have shown that phosphorylation of a specific serine (S) residues located in the N-terminal head domain mediates the interaction with 14-3-3 adaptors. The *14-3-3-Pred* software [41], which is effective at predicting the actual 14-3-3 binding sites in K17 and vimentin, predicts three potential binding sites in human K14 (S33, S44, S213), with S44 receiving the highest score. S44 in human K14 is orthologous to S44 in K17, previously shown to mediate 14-3-3σ binding [37]. Analyzing the mouse K14 sequence via *14-3-3-Pred* identifies S40 (Fig. 4A), which is orthologous to S44 in human K14, as the most probable 14-3-3 binding site. Finally, mass spectrometry analyses show that K14's S39 and S44 are phosphorylated in human N-TERT keratinocytes in culture (Suppl. Fig. 4A,B). With this information in hand, we generated two variants, one in which the "SCRAPS" motif in the N-terminal head domain of K14 is mutated to GFGGGS, the corresponding sequence in the N-terminal head domain of K15 (denoted K14-GFGGGS), and one in which K15's GFGGGS in K15 is replaced with K14's SCRAPS motif (Fig. 4A). Additional constructs generated included a A351C variant in human K15 (denoted K15-A351C) and the previously described C367A in human K14 (K14-C367A). This collection of mutants was utilized to compare K14's and K15's ability to regulate the subcellular distribution of YAP1 and their spatial proximity to 14-3-3 in transfected epithelial cells in culture [12].

The stutter cysteine and N-terminal SCRAPS motif cooperate to promote the keratin-dependent sequestration of YAP1 to the cytoplasm

Previously we utilized transfection-permissive HeLa cells to show that K14 mediates the cytoplasmic retention of YAP1 through, specifically, its stutter cysteine [12]. We returned to this system to assess the YAP1-modulating properties of co-expressed K14 and K15. Consistent with our previous findings [12], co-expression of mCherry-K5 WT (human) and EGFP-K14 WT (human) in HeLa cells enabled filament polymerization and resulted in localization of YAP1 to the cytoplasm and a decreased YAP1 nuclear:cytoplasmic ratio, as determined by a quantitative immunofluorescence assay (Fig. 4B; signal quantitation reported in Fig. 4C). By comparison, co-expression of mCherry-K5 (human), EGFP-K14 WT (human), and (untagged, mouse) K15 WT reduced the ability of K14 WT to redistribute YAP1 to the cytoplasm (Fig. 4B,C).

To test the hypothesis that K15's ability to reduce the K14-dependent cytoplasmic sequestration of YAP1 is dependent on its lack of a stutter cysteine, we co-expressed mCherry-K5 and EGFP-K14 with a stutter cysteine knock-in (A351C) mutant K15 in two contexts: the otherwise K15 wildtype sequence, and a K15 variant in which all other cysteines have been mutated to alanines (cysteine-free or CF). K15 CF functioned equivalently to K15 WT in its ability to repress K14-dependent YAP1 cytoplasmic sequestration (Fig. 4B, C). Remarkably, both K15 A351C and K15 CF A351C were unable to repress K14-dependent YAP1 cytoplasmic sequestration (Fig. 4B, C), suggesting that the stutter cysteine alone is sufficient to mediate YAP1 cytoplasmic sequestration.

We next sought to test the impact of K15 expression on K14-dependent relocalization of YAP1 to the cytoplasm in response to high calcium, a physiological trigger of differentiation, in mouse keratinocytes *ex vivo*. To do so we isolated primary keratinocytes from newborn *Krt14* $^{WT/null}$ hemizygous mouse pups and transfected them with EGFP-tagged (human) K14, K15, or K15 A351C overexpression vectors. Transfected cells were expanded for 2 days in calcium-free basal growth media before being switched to growth media containing 1.2 mM $CaCl_2$. Cells were calcium-differentiated for 24 hours, fixed, and stained for YAP1. As expected, nuclear YAP1 immunofluorescence signal decreased in mock (expressing endogenous K14 WT and K15 WT) and EGFP-K14 transfected keratinocytes following calcium-induced differentiation (Fig. 5A; quantitation shown in Fig. 5B). In agreement with the HeLa, *in vivo* morphological, and computational data presented earlier, EGFP-K15 transfection attenuated the calcium-induced reduction of nuclear YAP1 signal (Figs. 5A,B). Instead, overexpression of K15 in calcium-differentiating keratinocytes significantly increased nuclear YAP1 signal relative to EGFP-K15 expressing keratinocytes cultured under calcium-free conditions. In contrast, overexpression of knock-in stutter cysteine EGFP-K15 A351C resulted in loss of nuclear YAP1 signal in response to calcium as it did in mock and EGFP-K14 transfected cells (Figs. 5A,B). The data collected in

transfected HeLa cells and mouse keratinocytes in primary culture lead to the prediction that, in the human epidermis *in situ*, basal keratinocytes expressing K15 at higher levels should also exhibit stronger partitioning of YAP1 to the nucleus. Co-staining for K15 and YAP1 reveals a significant and positive correlation between K15 signal intensity and nuclear YAP1 signal intensity in sections of thin human skin epidermis (R^2=0.15, P<0.0001; Fig. 5C). Nuclear YAP1 signal intensity is, similarly to K15, strongest at the bottom of rete ridges (Fig. 5C). Together this in vitro, ex vivo, and in vivo data provides direct evidence that K15, through its lack of a stutter cysteine, maintains a progenitor cellular state by promoting nuclear YAP1 localization.

We next compared the ability of K14 and K15 mutants to promote spatial proximity between YAP1 and 14-3-3σ in transfected HeLa cells using proximity ligation assays (PLA). Here, we sought to functionally interconvert K14 and K15 by swapping the K14 SCRAPS motif and stutter cysteine with the orthologous residues in K15 (GFGGGS and A351). Co-expression of untagged K5 WT (human) and EGFP-K14 WT (human) in HeLa cells resulted in a robust PLA signal when probing for YAP1 and 14-3-3σ (Fig. 6A; signal quantitation reported in Fig. 6C). By comparison, co-expression of mCherry-K5 and either EGFP-K14-C367A, EGFP-K14-GFGGGS, or EGFP-K14-GFGGGS-C367A double mutant was ineffective at promoting YAP1/14-3-3σ physical proximity (Fig. 6A,B). These findings confirm our previous work focused on the K14 C367A variant and support the notion that the SCRAPS motif in K14's N-terminal head plays a role in the subcellular partitioning of YAP1 via 14-3-3σ interaction. By contrast, relative to EGFP-K14 WT, co-expression of K5 WT and EGFP-K15 WT (mouse) is as ineffective as EGFP-K14-C367A, EGFP-K14-GFGGGS, and EGFP-K14-GFGGGS-C367A at promoting YAP1/14-3-3σ physical proximity (Fig. 6A,B). Addition of both the SCRAPS motif and the stutter cysteine to K15 (EGFP-K15-SCRAPS-A351C double-mutant) proved necessary to functionally interconvert K15 and K14 in terms of YAP1/14-3-3σ PLA signal (Fig. 6A,B). While EGFP-K15-A351C was able to promote an intermediate level of YAP1/14-3-3σ proximity, EGFP-K15-SCRAPS was equivalent to EGFP-K15 WT. These findings suggest that the stutter cysteine and the SCRAPS motif function synergistically to promote a redistribution of YAP1 to the cytoplasm, and that WT K15's capacity to do so is significantly less because it lacks these two specific determinants.

K15 overrepresentation alters basal keratinocyte morphology and biases progenitor basal keratinocytes towards cell division

The experimental and computational data presented above provide evidence that keratinocytes with higher levels of K15, relative to K14, possess a stronger progenitor identity. To test this hypothesis *in vivo* we sought to manipulate the relative levels of K15 and K14

proteins in mouse skin. To do so we generated a mouse strain that exhibits compound heterozygous alleles at the *Krt14* locus - *Krt14*$^{C373A/null}$. This strain possesses a single allele of *Krt14* that is mutated at the stutter cysteine, while the *Krt15* alleles are unperturbed.

Krt14$^{C373A/null}$ mice are viable and blister-free (see below), indicating they express sufficient K14 to maintain epithelial integrity. To assess relative levels of K14 to K15, we performed quantitative dot blotting on whole tail skin lysate harvested from 8 week old male *Krt14*$^{C373A/null}$ mice, with their *Krt14*$^{C373A/WT}$ littermates used as control. *Krt14*$^{C373A/null}$ tail lysate displayed a significant 25.3% reduction in K14 mean steady state levels (Suppl. Fig 4C). K15, in contrast, was not significantly different between *Krt14*$^{C373A/WT}$ and *Krt14*$^{C373A/null}$ samples (Suppl. Fig 4C), confirming the alteration to the K14 to K15 ratio in *Krt14*$^{C373A/null}$ skin.

In the progeny resulting from crosses between *Krt14* $^{C373A/C373A}$ and *Krt14*$^{WT/null}$ mice, we noticed that a subset of pups, by P4, had a plumper, darker and slightly larger appearance as the first group of hair follicles completes differentiation and fur emerges at the skin surface (Fig. 7A). Upon weighing, such pups were on average 10% heavier than their littermates (3.02g vs. 2.75g). Genotyping performed at weaning indicated that these features were completely specific to the *Krt14*$^{C373A/null}$ genotype, with no sex bias. The difference in body weight does not persist after pups are weaned, such that *Krt14*$^{C373A/null}$ and *Krt14*$^{C373A/WT}$ mice are indistinguishable as young adult mice.

The gross appearance of the *Krt14*$^{C373A/null}$ pups suggested that they may exhibit thicker skin, a suspicion that was confirmed through routine histology. The increase in *Krt14*$^{C373A/null}$ skin thickness was most significant in the dermis, and correlated with a general increase in hair follicle length (by 19%, on average; Fig. 7B'). The latter is consistent with the observation, reported above, that hair erupts a day earlier in *Krt14*$^{C373A/null}$ relative to *Krt14*$^{C373A/WT}$ littermates. Quantitation showed that the interfollicular epidermis was also thickened, by 35%, in the *Krt14*$^{C373A/null}$ pups (Fig. 7B'). Upon closer examination, additional alterations were observed in the epidermis of hematoxylin-eosin stained sections of *Krt14*$^{C373A/null}$ skin at 8 weeks. In the upper epidermis of the tail, the granular compartment was decreased in both density and contrast while the cornified layers were expanded, respectively suggesting mild alterations in terminal differentiation and mild hyperkeratosis (Fig. 7C). In the lower epidermis, basal keratinocytes appeared crowded and showed clustering in *Krt14*$^{C373A/null}$ mice whereas they were evenly distributed along the basal lamina in *Krt14*$^{C373A/WT}$ controls (Fig. 7C). Areas with nuclear clustering displayed muddled H&E staining (Fig. 7C). To quantitate these features, we measured the mean surface area of basal keratinocytes and their density per unit length of dermo-epidermal interface. The mean area of *Krt14*$^{C373A/null}$ basal keratinocytes was significantly

smaller than *Krt14*$^{C373A/WT}$ basal keratinocytes in tail epidermis (*Krt14*$^{C373A/WT}$: 71.50 μm^2 vs. *Krt14*$^{C373A/null}$: 66.70 μm^2; Fig. 7D). In concurrence, the density of basal keratinocytes per μm of dermo-epidermal interface was significantly increased in *Krt14*$^{C373A/null}$ keratinocytes (*Krt14*$^{C373A/WT}$: 0.1324 cells/μm vs. *Krt14*$^{C373A/null}$: 0.1616 cells/μm, Fig. 7E).

To test whether basal cell crowding in adult *Krt14*$^{C373A/null}$ epidermis was associated with increased cell divisions, we performed Ki67 immunofluorescence staining, a highly specific marker for cycling cells, on tail skin harvested from 8 week old *Krt14*$^{C373A/WT}$ and *Krt14*$^{C373A/null}$ male and female littermates. As expected, Ki67 staining is exclusively localized to the basal keratinocytes in both *Krt14*$^{C373A/WT}$ and *Krt14*$^{C373A/null}$ tissue. *Krt14*$^{C373A/null}$ tissue, however, showed a significant increase in Ki67 mean intensity value in basal nuclei (Fig. 7F). We next set a threshold for Ki67 positivity by determining the median Ki67 intensity for nuclei that were visually negative for Ki67 and calculated the percentage of basal cells above this threshold. In *Krt14*$^{C373A/WT}$ basal keratinocytes, 6.8% of nuclei were Ki67-positive, while 16.8% of *Krt14*$^{C373A/null}$ basal keratinocyte nuclei were Ki67-positive (Fig. 7G). Both parameters confirm an increase in Ki67-positive nuclei in 8 week old *Krt14*$^{C373A/null}$ tail tissue compared to *Krt14*$^{C373A/WT}$ littermates.

Finally, we used transmission electron microscopy (TEM) to identify any ultrastructural alterations in *Krt14*$^{C373A/null}$ epidermis. We imaged skin dissected from the back, ear, and tails of 8 week old, male and female, *Krt14*$^{C373A/null}$ and *Krt14*$^{C373A/WT}$ littermates (Fig. 7H). Recurring observations from *Krt14*$^{C373A/null}$ skin include alterations to nuclear morphology and an increased incidence of cytoplasmic regions devoid of keratin filaments (see “Nu” and asterisks in Fig. 7H). The basal lamina in *Krt14*$^{C373A/null}$ basal keratinocytes also displays an increase in its spatial convolution and its thickness (Fig. 7I). Additional recurrent features specific to *Krt14*$^{C373A/null}$ basal keratinocytes include more prominent hemidesmosomes, typically associated with distortions in the basal lamina, along with cytoplasmic regions devoid of keratin filaments (Fig. 7H; see “kf”). These ultrastructural studies show that an increased K15:K14 ration (see Suppl. Fig. 4C) is associated with alterations to the morphological attributes of basal keratinocytes, basal lamina, and hemidesmosome adhesions.

DISCUSSION

A link between K15 expression and an epithelial stem character was first uncovered in the human hair bulge by Lyle et al. >25 years ago [9]. This link has since been confirmed and expanded to mouse skin [42] and to internal stratified epithelia, such as the esophagus [11] (see review by [10]). Follow-up studies, in human and in mouse, have shown that *Krt15*^{high}-expressing keratinocytes residing in the basal layer (and purified based on high surface levels of integrins)

express several markers associated with stemness (e.g., CD34, CD200, integrin B1^{bright}, Lgr5; see [43-47]) and are fully capable of reconstituting all epithelial lineages in-mature hair follicles [44] and esophagus [11]. By contrast, *Krt15^{low}*-expressing, basally-located keratinocytes (which are otherwise *Krt14^{high}* in character) do not exhibit this lineage potential [44]. In human epidermis, K14 and K15 are co-expressed in basal layer keratinocytes at the transcript and protein levels, but the distribution of K15 is unique in many respects; unlike K14, K15 occurs in a subset of basal keratinocytes that are preferentially located in the deeper area of epidermal rete ridges, and it does not persist in suprabasal keratinocytes [19,20,26-29]. We confirmed and significantly extended these observations, e.g., through a comprehensive analysis of single cell transcriptomics data. As intriguing as these attributes are, however, there is, as of yet, no biochemical or mechanistic insight that accounts for the intriguing connection between K15 expression and an epithelial stem character in skin.

Here, we report on findings establishing that, owing to the lack of two key cis-acting determinants - a cysteine within the stutter motif of the α-helical central rod domain and a 14-3-3 binding motif in the N-terminal head domain - K15 is unable on its own to effectively mediate the cytoplasmic sequestration of YAP1. Accordingly, and unlike K14 [12], K15 is unable to enact a switch in Hippo signaling, from “off” to “on”, that prompts progenitor basal keratinocytes to initiate differentiation in the epidermis. **Figure 8** illustrates a model that integrates these new findings with previous work focused on the K14/14-3-3σ/YAP1 interaction [12]. The model proposes that a higher K15:K14 protein ratio in basal keratinocytes of epidermis promotes the progenitor state and antagonizes differentiation. Once *KRT15* expression subsides and the K15:14 protein ratio falls below a postulated threshold (a reality favored by K15’s apparent shorter half-life [48] along with persistence of *KRT14* expression at significant levels), K14 is able to effectively sequester YAP1 to the cytoplasm and promote entry into differentiation. Our model further proposes that the YAP1 sequestering role of K14 is amplified and maintained by the subsequent expression of the differentiation-related K10 in interfollicular epidermis. K10, like K14, engages in trans-dimer disulfide bonding through its stutter cysteine [14] and binds 14-3-3σ [49,50]. Further, as pointed out before [12], suprabasal keratinocytes in the epidermis of *Krt10* null mice [51] exhibit clear signs of persisting YAP1-dependent cell proliferation and gene expression. More broadly, we propose a new conceptual framework stating that the sequential expression of K15, K14 and K10 in epidermal keratinocytes of human thin skin (see Fig. 2) acts to: i) maintain the progenitor state, via K15; ii) mediate entry into differentiation, via a modified form of K14; and iii) maintain an active differentiating state, again via a modified form of K10. The sequential roles of K14 and K10 in promoting keratinocyte differentiation entails their interaction with 14-3-

3σ. Computational analysis of human foreskin single cell data argues that the model we propose likely applies to other stratified epithelia that co-express K14 and K15.

With the notable exception of *KRT15,* initial insight about the functional importance of the keratin genes expressed in the epidermis was inferred from the phenotype of transgenic mouse models and/or individuals suffering from rare genetic skin disorders. The main disorder associated with *KRT14* (and *KRT5*), EBS, is typically caused by dominantly-acting missense alleles [7] but also arises in individuals whose genome is homozygous for null alleles [19,21,52]. No disease association has been reported yet for *KRT15*. Yet, GnomAD [53] reports variants at several codons in *KRT15*, with many alleles predicted to act deleteriously including those altering arginine 115. The latter corresponds to a prominent mutational hotspot in *KRT14* (Arg-125; [7]) and other type I keratin genes expressed in healthy epidermis, including *KRT10* and *KRT9* [54,55], and is consistently associated with severe clinical presentations. Per GnomAd [53], Arg 115 in *KRT15* is mutated at an appreciable frequency in the human population and yet no disease association has been reported. Moreover, mice null for *Krt15* are viable and do not exhibit skin fragility (see below) whereas mice null for *Krt14* [23] or *Krt5* [56] show extensive and penetrant skin and oral blistering, and die postnatally. At least two known factors likely account for these striking differences. First, K15 is expressed at lower levels than K14 (and K5) in basal keratinocytes – this is so at the transcript level in human and mouse epidermis (this study) and at the protein level in newborn mouse skin [57] – such that the consequences of its mutated form may be mitigated by the presence of K14 at higher levels. Second, K15 expression is highest in basal cells located in the deeper segments of epidermal rete ridges – accordingly, they may be protected from frictional trauma and, transcriptionally, they exhibit higher expression of genes mediating adhesion to the ECM (this study; see [44,45]). As a non-exclusive, third possibility, it may be that incorporation of K15 into the keratin filament network of basal keratinocytes does not enhance mechanical properties as readily as incorporation of K14 does [58]. At present, therefore, *KRT15*/K15 stands out among the main epidermal keratins given a lack of known involvement in a human genetic disease.

Mice in which the *Krt15* locus has been targeted for inactivation have been reported [48,59] but a detailed characterization of their skin phenotype is not available. *Krt15* null mice are viable and, while they do not show any sign of epithelial fragility, they exhibit patchy hair loss as young adults [48,59]. The latter could reflect a hair cycle defect and/or a premature exhaustion of the hair bulge-associated stem cell pool, a possibility consistent with our model. While it was focused on studying the trachea, which features a pseudostratified epithelium, the effort by levlev et al. [59] yielded findings that directly support our model. These authors showed that mice targeted at the

Krt15 locus exhibit impaired basal cell proliferation in the airways but did not show alterations in their subsequent differentiation. By contrast, mice targeted at the *Krt14* locus in a similar manner show enhanced proliferation of basal cells along with impaired differentiation into ciliated and club cell types. levlev et al. [59] also observed a decrease in label-retaining basal cells in the tracheal epithelium at 21 days after injury in *Krt15* null mice. Although the strategy used by these authors to target the *Krt14* or *Krt15* loci may not have yielded truly null alleles (they deleted exon 3, which codes for the C-terminal half of coil 1B in the central rod domain of K14, K15), the findings reported are entirely consistent with ours and strongly support for our model.

In our study, we reasoned that a distinct approach in which the K14:K15 ratio is altered, the function of K14's stutter cysteine is negated and the occurrence of EBS-like cell fragility is avoided would provide an effective test of our model in skin tissue. The *Krt14*$^{null/C373A}$ compound heterozygous mice that we generated and characterized are viable and skin blister-free, as expected. Interestingly, they exhibit premature growth and differentiation of hair follicles and epidermis as early postnatal traits, along with hyperkeratosis, modestly enhanced proliferation, basal cell crowding, and ECM alterations in the epidermis, again consistent with our model.

How K15 promotes the progenitor state in the epidermis, e.g., whether it goes beyond hampering K14's ability to negatively regulate YAP1's transcriptional role, is unknown. The evidence in hand does not support a direct role for K15 in cell cycle control (similarly to K14; see [5,32]). In skin, *KRT15*^{high} keratinocytes occur infrequently in G2/M-phase^{high} or S-phase^{high} subpopulations (this study; also, see [43,44]). We envision that a higher K15:K14 keeps keratinocytes in a progenitor state in which they remain sensitive to proliferation cues. This interpretation is consistent with the original description of K15 as being enriched in slow-cycle keratinocytes of the hair bulge [9]. On the other hand, we show here that *KRT15* (in the human) and *Krt15* (in the mouse) are, at the single cell level, highly positively correlated with genes that define the relationship with the extracellular matrix. Remarkably, many of these genes are known YAP1 targets (e.g., *CYR61*, *CCND2*, *TGFB1*) and/or have been implicated in fostering a microenvironment ("niche") that promotes epithelial stemness (e.g., *COL17A1*, *ITGA1*, *POSTN*) [44,45]. We showed that the ultrastructural attributes of the basal lamina and, more generally, of the basement membrane zone are markedly altered in *Krt14*$^{null/C373A}$ mice, consistent with alterations in mechanosensing and/or mechanotransduction and in proliferation. The size of keratinocytes and the morphological attributes of the nucleus in the basal layer of *Krt14*$^{null/C373A}$ epidermis are altered as well (see [59] for similar findings). How these differences arise, molecularly, is unknown at this point. Previous studies have described a conspicuous lack of keratin bundling and the presence of so-called "wispy" keratin filaments in basal keratinocytes of *KRT14* null human

[19,21,52] and *Krt14* null mouse skin [23]. While this may be a function of the lower prevailing levels of K15 protein in such circumstances, our own comparison of cells that were transfected with K14 vs. K15 supports the notion that these two homologs may promote the formation of filaments having different properties. The stutter cysteine may play a role in this regard, as suggested by our observations of epithelial cells engineered to express WT K15 vs. K15 A351C.

The success of our mutagenesis efforts in interconverting K14's and K15's properties to a significant degree highlight a dominant role for the stutter cysteine in enabling select keratin proteins to regulate YAP1 in the skin keratinocytes. Another type I keratin associated with a stem-like epithelial character in skin [60], namely K19, also lacks the stutter cysteine [12,13]. Also of interest, select differentiation-related keratins in internal epithelia, including K13 characteristic of the oral mucosa and esophagus (see Uniprot database [61]), also lack the stutter cysteine. Future efforts should be aimed at defining when and how, precisely, K14 and other stutter cysteine-containing keratins engage 14-3-3 adaptors and YAP1, and how cysteines occurring at other positions within K14 [12] and other keratin proteins modulate their properties and cellular roles.

ACKNOWLEDGMENTS

The authors are grateful to members of the Coulombe laboratory for advice, to Beau Su for logistical support, and to Venkatesha Basrur (Proteomics Resource Facility), Anna LaForest and Corey Ziebell (Transgenic Core Facility), and Woo Jung Cho and Devon Leroux (Microscopy Imaging Laboratory) at the Univ. Michigan Medical School for technical assistance. CJR (F99 CA274517), SNS (F31 AR038249) and EC (T32 AR007197) received fellowship awards from the National Institutes of Health. EC also received fellowship support from the National Psoriasis Foundation. These studies were supported by grant R01 AR0079418 to PAC from the NIH.

AUTHOR CONTRIBUTIONS

Conceptualization: CJR and PAC, with input from EC and SNS.
Methodology: CJR, SNS, EC, NO, CNJ and PAC.
Investigation: CJR, SNS, EC, and NO. Writing - original draft: CJR and PAC.
Writing, review and editing: CJR, SNS, EC, NO, CNJ and PAC.
Resources: PAC.
Supervision: PAC and CJR.

DECLARATION OF INTERESTS

None of the authors has a conflict of interest to declare.

METHODS

Mouse studies

All mouse studies were reviewed and approved by the Institutional Animal Use and Care Committee (IACUC) at the University of Michigan. All mice (C57BL/6 strain background) were maintained under specific pathogen-free conditions, fed rodent chow and water ad libitum, and kept under a 12-h day/night cycle. Male and female C57Bl/6 mice of 2–3 months of age (young adults) were used for all studies unless indicated otherwise. *Krt14*$^{C373A/C373A}$ mice were previously reported in [12]. Cryopreserved sperm from *Krt14*$^{WT/null}$ mice was purchased from MMRRC (Strain name: C57BL/6N-Krt14 /MbpMmucd tm1.1(KOMP)Vlcg; RRID:MMRRC_048362-UCD). In vitro fertilization of eggs harvested from C57Bl/6 females was performed by the University of Michigan Transgenic Core. Pups were screened for the null allele using standard PCR assays with oligonucleotides listed in STAR*Methods, and a transgenic line was established and maintained (C57BL/6 background) through standard husbandry methods.

K14 and K15 amino acid alignment and 14-3-3 binding site prediction

Sequence alignments were performed using the Clustal Omega freeware in the UniProt alignment tool on human *KRT14* and *KRT15* and mouse *Krt14* and *Krt15*. Computational predictions for 14-3-3 binding were performed using the 14-3-3pred freeware (https://www.compbio.dundee.ac.uk/1433pred).

YAP1 indirect immunofluorescence and quantitation of nuclear:cytoplasmic signal ratio

HeLa cells were purchased from ATCC and were routinely tested for mycoplasma using the MycoAlert® Mycoplasma Detection Kit (Lonza, LT07-118). Cells were cultured in 4.5 g/L D-glucose DMEM (Gibco, 11995073) supplemented with 1% penicillin and streptomycin (Gibco, 15140122) and 10% fetal bovine serum. TWIST mammalian expression plasmids were synthesized by Twist Biosciences (San Francisco, CA). Codon-optimized *KRT14* and *KRT15* cDNAs were synthesized into a pTwist-CMV vector containing a CMV enhancer and promoter for expression in mammalian cells. All plasmids were verified by whole plasmid sequencing (Plasmidsaurus). HeLa cells were transfected using the SE Cell Line 4D-Nucleofector kit (Lonza, V4XC-1032) and program DS-138. 300,000 cells and a total of 2 μg of plasmid DNA were transfected per parameter. After transfection, cells were plated on #1.5 glass coverslips and cultured for 24 h. After 24 h, media was removed, and cells were fixed in 4% PFA/PBS for 10 min. Fixed cells were washed, permeabilized for 5 min in 0.1% Triton X-100, and then incubated for 1 h with rabbit anti-YAP1 antibody (Cell Signaling Technology, 14074S), followed by 1 h incubated with an Alexa Fluor conjugated secondary antibody, and counterstained with DAPI. Coverslips were mounted on a slide with Fluorsave (Millipore, 345789). Coverslips were imaged with a 63X objective with a Zeiss LSM 800 confocal microscope. Laser intensity and detector gain were optimized for each fluor/channel. YAP1 localization was quantified using Zeiss ZEN Lite software. Using the spline tool, the cytoplasm (defined by the mCherry channel) and the nucleus (defined by the DAPI channel) were traced. The area and mean intensity values (MIV) for each channel were calculated for the cytoplasmic and nuclear objects. The cytoplasmic object also contains the nuclear object. The sum intensity value (SIV) of YAP1 was calculated by multiplying the area by the mean intensity value for the cytoplasmic and nuclear objects. The nuclear YAP1 sum intensity value was subtracted from the cytoplasmic YAP1 sum

intensity value. The MIV of the resultant nuclear subtracted cytoplasmic SIV was calculated by dividing by the nuclear area subtracted from the cytoplasmic area. The Nuclear:Cytoplasmic YAP1 ratio was calculated for each cell and controlled for transfection by correction and normalization for 488 channel intensity. Statistical analysis was performed in GraphPad Prism. Conditions were compared with Mann-Whitney tests. For figure visualization, datapoints were normalized to the mean of the “K5/no plasmid” sample condition.

YAP1-14-3-3σ proximity ligation assay (PLA) and quantitation

pMAX-GFP was supplied from Lonza. All keratin overexpression constructs were synthesized by Twist Biosciences and subjected to whole plasmid sequencing (Plasmidsaurus). HeLa cells were transfected using SE Cell Line 4D-Nucleofector kit (Lonza, V4XC-1032) and program CN-114. 150,000 cells and 1 ug of total plasmid DNA were transfected per parameter. After transfection, cells were plated on #1.5 glass coverslips and cultured for 24 h. After 24 h, media was removed, and cells were rinsed with 1X PBS and fixed in 4% PFA/PBS for 10 min. Fixed cells were washed, permeabilized for 10 min in 0.1% Triton X-100, and then blocked in 2.5% NDS/PBS overnight at 4C. Cells were then incubated for 1 h at 37C with rabbit anti-YAP1 antibody (Cell Signaling, 14074S) and goat anti-14-3-3σ antibody (Abcam, ab77187). Following primary antibody incubation, cells were incubated with anti-rabbit PLUS and anti-goat MINUS DuoLink Probes (Sigma-Aldrich, DUO92002, DUO92006), and PLA signal was developed according to manufacturer protocol (Sigma-Aldrich, DUO92013). Coverslips were imaged with a 40X objective with a Zeiss LSM 800 confocal microscope. Laser intensity and detector gain were optimized for each fluor/channel. Images were taken as Z-stacks spanning 10μm at 1μm intervals. ImageJ was used to generate maximum intensity projection images, and PLA punctae/cell were quantified using the ImageJ multi-point tool, using GFP autofluorescence to define the boundaries of the cell(s).

Human buttocks skin indirect immunofluorescence

Sections of paraformaldehyde-fixed, paraffin-embedded healthy human buttocks skin was provided by Dr. Johann Gudjonsson’s laboratory (Department of Dermatology, University of Michigan Medical School) as part of a IRB-approved protocol (see [30]). Sections were deparaffinized in Histo-Clear (National Diagnostics, HS-200), and rehydrated in (2x) 100% EtOH, 95% EtOH, 70% EtOH, and running distilled water. Slides were blocked in 2% normal donkey serum/1% BSA/PBS for 1 hour at RT, incubated in primary antibody diluted in blocking solution (1:200, chicken anti-keratin 14 (BioLegend, 906004); 1:200 chicken anti-keratin 15 (BioLegend, 833904)) for 16 h at 4 ºC, Alexa Fluor-conjugated secondary antibody for 1 h at 37 ºC, counterstained with DAPI, and mounted in Fluorsave (Millipore, 345789) and a #1.5 cover-slip. Slides were imaged with a 40X objective with a Zeiss LSM 800 confocal microscope. Laser intensity and detector gain were optimized for each fluor/channel. Scale bar represents 50 μm.

Isolation of newborn skin keratinocytes for primary culture

Newborn mouse keratinocytes were harvested from P0, P1, and P2 pups and seeded in primary culture as follows (see [12]). Pups were decapitated, sterilized in 10% (w/v) Povidone-Iodine Solution (Fisher Scientific, 3955-16), and rinsed in 70% EtOH and distilled water. Back skin was dissected and suspended for 18 h in 0.25% Trypsin-EDTA (Gibco, 25200056) at 4 ºC. The epidermis was then removed from the dermis and placed basal layer side up in a cell culture

dish lid. The living keratinocytes were carefully scraped from the waxy cornified layer and resuspended in basal medium (calcium-free DMEM (US Biological, D9800-10, 70% v/v), Ham's F-12 (Gibco, 11765054, 22% v/v), Chelex-treated FBS (Bio-Rad, 1421253, 10% v/v), adenine (Sigma-Aldrich, A8626-5G, 0.18 mM), hydrocortisone (Sigma-Aldrich, H4001-1G, 0.5 ug/mL), insulin (Sigma-Aldrich, I9278, 5 ug/mL), cholera toxin (ICN, 856011, 10 nM), EGF (Sigma-Aldrich, E4127, 10 ng/mL), GlutaMAX (Gibco, 35050061, 2 mM), sodium pyruvate (Gibco, 11360070, 1 mM), penicillin (Sigma-Aldrich, P3032-1MU, 100 U/mL)). Pooled back skin keratinocytes were then layered on top of Lymphoprep (Stem Cell Technologies, 07851) and spun for 30 min at 800 x g. The top layer of basal media, containing living cells, was then removed and respun to pellet. The pelleted cells were resuspended in fresh basal media, plated onto #1.5 coverslips, and cultured for up to 72 h. For fixation, media was removed from cells, replaced with 4% PFA/PBS for 10 min, followed by 4 rinses with 1X PBS.

Transfection and calcium switching of mouse skin keratinocytes in primary culture
Primary cultures of keratinocytes were established as described above. Prior to plating, skin keratinocytes were transfected using P3 Primary Cell 4D-Nucleofector™ X Kit (Lonza, V4XP-3032) and program DS-138. Codon optimized *KRT14* and *KRT15* cDNA was synthesized into a EGFP-C3 vector containing a CMV enhancer and promoter for expression in mammalian cells Twist Biosciences; see above). 0.5 ug of DNA was transfected per parameter. After transfection, cells were plated on #1.5 glass coverslips and cultured for 48 h. Cells were then calcium differentiated by removing media and replacing with basal media supplemented with calcium chloride (Sigma-Aldrich, C7902, 1.2 mM) for 24 h. Cells were fixed by removing the media and replacing with 4% PFA/PBS for 10 min, then rinsed 4x with 1X PBS.

Indirect immunofluorescence for nuclear YAP1 and its quantitation
Transfected keratinocytes in primary culture were fixed, washed, permeabilized for 5 min in 0.1% Triton X-100, and incubated in primary antibody diluted in 5% NDS/1X PBS blocking buffer (1:100, rabbit anti-YAP1 (Cell Signaling Technology, 14074)) for 1 h at 37 ºC, followed by 1 h at 37 ºC in an Alexa Fluor conjugated secondary antibody diluted in PBS, and counter-stained with DAPI. Coverslips were mounted on a slide with Fluorsave (Millipore, 345789). Coverslips were imaged using a 40X objective fitted on a Zeiss LSM 800 confocal microscope. Laser intensity and detector gain were optimized for each fluor/channel. YAP1 intensity mean value was quantified using Zeiss ZEN Lite software. Using the spline tool, the nuclei of EGFP-keratin fluorescing cells was traced and the YAP1 mean intensity value was calculated.

Indirect immunofluorescence for K14 and K15 on primary keratinocytes and quantitation
Fixed cells were washed, permeabilized for 5 min in 0.1% Triton X-100, and then incubated in primary antibody diluted in 5% NDS/1X PBS blocking solution (1:200, chicken anti-keratin 14 (BioLegend, 906004); 1:200 chicken anti-keratin 15 (BioLegend, 833904)) for 1 h at 37 ºC, followed by 1 h at 37 ºC in an Alexa Fluor conjugated secondary antibody diluted in PBS, and finally counterstained with DAPI. Coverslips were mounted on a slide with Fluorsave (Millipore, 345789). Coverslips were imaged with a 63X objective with a Zeiss LSM 800 confocal microscope. Laser intensity and detector gain were optimized for each fluor/channel. K14 and K15 intensity mean value were quantified using Zeiss ZEN Lite software. Using the spline tool, the cytoplasm was traced and the mean intensity values for each channel were calculated.

There were no apparent alterations to keratin filament morphology, emulating previous observations in *Krt14*$^{C373A/C373A}$ primary keratinocytes [12].

Seurat clustering

Single cell RNAseq datasets from human trunk skin and foreskin were originally published by Cheng et al. [62]. The data was reanalyzed using Seurat's SCTransform "v2" as detailed in a previous publication [30]. Analysis For the single cell RNAseq dataset from saline-treated mouse back skin (GSE194254) [63] were done as follows: cells were filtered to remove doublets using scDblFinder [64], percent mitochondrial genes (<15%) and number of features (400< x <4000). Retained cells (12,093 cells) were then processed using harmony to integrate 20 principal components and perform dimensional reduction, with 0.5 resolution for clustering. This analysis resulted in the identification of 22 unique clusters. Enrichr [65] was used to analyze the Seurat clusters for keratinocyte gene signatures using PanglaoDB dataset [66], identifying 7 keratinocyte cell clusters used for further analysis (4,806 cells). Data clustering and analysis was performed using R version 4.4.1, and Seurat version 5.

Generation of Transcription Signature Composite Scores

Composite scores (Differentiation score, Basal score, G2M Score, S Score) were calculated using arithmetic mean of Seurat normalized natural log values. The following genes (and their direct mouse orthologues) were included in composite scores as follows:

Basal score: *POSTN, ITGB1, LAMA5, COL17A1,DST.*
Differentiation score: *DSP*, *DMKN*, *KRTDAP*, *DSG1*, *SBSN*.
G2M Score: *MKI67*, *TOP2A*, *CDC20*, *BUB3*, *CCNB2*.
S Score: *RPA2, UHRF1, ATAD2, RFC2, RRM2*

These scores have been previously shown to accurately represent the cellular states and transitions across epidermal keratinocyte differentiation [5,30]. A difference score between basal and differentiation ('Differentiation Score -Basal Score') was used to organize keratinocyte clusters according to their natural continuum when analyzing keratin level per cluster (Figure2, SuppFigure2 and SuppFigure3). Last, expression of individual keratin genes *(KRT14*, *KRT15*, *KRT10*, *KRT2*), was analyzed against composite scores on a Seurat cluster or single-cell level. Graphs and statistical analysis were generated using Graphpad Prism 9.1.0, and the statistical methods used are reported within figure panels.

Pup observations, weights, and histological analysis

Pups born from crosses of *Krt14*$^{C373A/C373A}$ and *Krt14*$^{null/WT}$ were observed daily for 3 weeks. In the first postnatal week, pups were not touched. Observations were performed through the cage so as not to disturb the breeding pair. After week 1, the nest was moved to take pictures of the pups. Between weeks 2 and 3, pups were weighed daily in the afternoons in a weigh boat using a small scale. Pups were tracked based on unique identifying tail markings. For histological analysis, pups were euthanized via decapitation. Back skin was harvested and submerged overnight in an excess of 10% neutral buffered formalin. After fixation, tissue was arranged into cassettes, stored in 70% EtOH at RT, and handed to the University of Michigan Department of Pathology Research Histology Core for paraffin embedding and sectioning. FFPE tissue was deparaffinized in Histo-Clear (National Diagnostics, HS-200), and rehydrated in (2x) 100% EtOH, 95% EtOH, 70% EtOH, and running water. Hematoxylin (Thermo Scientific, TA-060-MH)

and eosin Y (Thermo Scientific, 71204) staining was performed per Sigma-Aldrich Procedure No. MHS #1. Epidermal thickness was quantified in ImageJ by measuring from bottom of the basal layer to the top of the granular layer perpendicular to the basal lamina at the point. Measurements were collected every 15 µm of basal lamina. Hair follicle length was quantified in ImageJ by measuring from the bottom of the hair follicle bulb to the basal layer of the infundibulum. Only hair follicles with visible bulbs were measured. Statistical analysis was performed in GraphPad Prism. Conditions were compared with Mann-Whitney tests.

Dot blot analysis of skin tissue proteins

Tail skin (roughly 1 inch in length, towards the base of the tail) was harvested from 8 week old, male and female, *Krt14*$^{C373A/WT}$ and *Krt14*$^{C373A/null}$ littermates. Skin was finely minced with fresh razorblades and nutated for 24 h at 4 ºC in urea lysis buffer (pH 7.0, 6.5M urea (Sigma-Aldrich, U5378), 50 mM Tris-HCl, 150 mM sodium chloride, 5 mM ethylenediaminetetraacetic acid (EDTA), 0.1% Triton X-100, cOmplete Proteinase Inhibitor Cocktail (Roche, 11697498001)). Tissue was then homogenized on ice with a probe homogenizer and spun at 16,200 x g for 30 min at 4 ºC. The insoluble pellet was discarded, and protein concentration of the supernatant was determined by BCA assay (Thermo Scientific, 23225). Dot blotting was performed using a 96-well Minifold I Dot-Blot System (Cytiva, 10447900). Samples were eluted through a 0.45 µm nitrocellulose membrane (BioRad, 1620115) overlaying thick pure cellulose chromatography paper (Fisher Scientific, 05-714-4). Membrane and paper were pre-wet with 3 washes of PBS. Wells were preloaded with 200 µL of 0.01% BSA/PBS. 7.5, 5, 2.5, 1, and 0.5 µg of lysate was added directly to 0.01% BSA/PBS. Samples were eluted and vacuum remained on for 5 min to dry the membrane. Membranes were blocked in 5% BSA/PBS for 1 h following transfer. After blocking, membranes were cut and incubated in primary antibody (1:1000 rabbit anti-histone H3 (Abcam, ab1791); 1:1000 chicken anti-keratin 14 (BioLegend, 906004); 1:1000 chicken anti-keratin 15 (BioLegend, 833904)) diluted in 5% BSA/PBS blocking buffer overnight at 4 ºC. Membranes were washed in PBS-T, incubated for 1 h at RT in HRP-conjugated secondary antibodies, and washed prior to visualization with ECL (Cytiva, RPN2232). Mean gray values (MGV) of dots were quantified using ImageJ elliptical selection tool and measurement function. K14 and K15 MGV were normalized for loading by dividing by histone H3 MGV. For data visualization, MGV of each datapoint (corresponding to a single dot) were divided by the mean of the *Krt14*$^{C373A/WT}$ populations.

Histological analysis and quantification of basal keratinocyte density

At 8-weeks of age, male and female *Krt14*$^{C373A/null}$ animals appeared healthy and were indistinguishable from *Krt14*$^{C373A/WT}$ control littermates. Tissue was harvested from the tail, ear, and tongue and immediately frozen at -40 ºC in Tissue-Tek OCT compound (Sakura, 4583). Hematoxylin (Thermo Scientific, TA-060-MH) and eosin Y (Thermo Scientific, 71204) staining was performed on fresh, frozen tissue. 5 µm sections were placed onto slides and air dried for 10 min. Hematoxylin and eosin Y staining was performed per Sigma-Aldrich Procedure No. MHS #1. Basal cell crowding was quantified on skin sections of paraformaldehyde-fixed, paraffin embedded (FFPE) tissue. Tail skin was dissected from 8 week old, male and female, *Krt14*$^{C373A/WT}$ and *Krt14*$^{C373A/null}$ littermates. Harvested tissue was fixed for 18 h at 4 ºC in 10% neutral buffered formalin (Sigma-Aldrich, HT501128). After fixation, tissue was arranged into cassettes, stored in 70% EtOH at RT, and handed to the University of Michigan Department of

Pathology Research Histology Core for paraffin embedding and sectioning. FFPE tissue was deparaffinized in Histo-Clear (National Diagnostics, HS-200), and rehydrated in (2x) 100% EtOH, 95% EtOH, 70% EtOH, and running water. Slides were blocked in 5% normal donkey serum/1% BSA/PBS for 1 h at RT, incubated in primary antibody (1:200, chicken anti-keratin 14 (BioLegend, 906004); 1:200, chicken anti-keratin 15 (BioLegend, 833904)) for 16 h at 4 ºC, Alexa Fluor-conjugated secondary antibody for 1 h at RT, counterstained with DAPI, and mounted in Fluorsave (Millipore, 345789) and a #1.5 coverslip. Slides were imaged with a 40X objective with a Zeiss LSM 800 confocal microscope. Laser intensity and detector gain were optimized for each fluor/channel. Area was calculated by tracing individual basal keratinocytes. The cytoplasm was distinguished by K15 immunofluorescence staining. K15 is a suitable for this purpose as it is a pan-cytoplasmic stain with distinct gaps at cell peripheries. To calculate basal cell density, basal lamina distance was measured and cells along this distance were counted. Statistical analysis was performed in GraphPad Prism. Conditions were compared with Mann-Whitney tests.

Ki67 indirect immunofluorescence and quantitation

Tail skin was dissected from 8-week-old male and female *Krt14*$^{C373A/WT}$ and *Krt14*$^{C373A/null}$ tail skin processed for FFPE, and immunostained, as described above. Slides were blocked in 5% normal donkey serum/1% BSA/PBS for 1 h at RT, incubated in primary antibody (rabbit anti-Ki67 (Cell Signaling Technology, 9129S); chicken anti-keratin 15 (BioLegend, 833904)) for 16 h at 4 ºC, Alexa Fluor-conjugated secondary antibody for 1 h at room temperature, counterstained with DAPI, and mounted in Fluorsave (Millipore, 345789) and a #1.5 coverslip. Slides were imaged with a 40X objective with a Zeiss LSM 800 confocal microscope. To quantify Ki67 intensity and positivity, the nucleus of individual basal keratinocytes was traced in ZEISS ZEN Lite using the spline tool. The nucleus was distinguished by DAPI immunofluorescence staining. The intensity mean values for each channel per traced cell were then measured. Statistical analysis (Mann-Whitney test) and visualization were performed using GraphPad Prism. The mean Ki67 intensity (arbitrary units) was compared for the entire population of nuclei between *Krt14*$^{C373A/WT}$ and *Krt14*$^{C373A/null}$ samples. To calculate the percentage of Ki67 positive nuclei, a threshold for Ki67 positivity was determined by selecting a population of nuclei with the visually lowest, to absence of, Ki67 signal. The median Ki67 intensity of this population was determined to be 7000 arbitrary units. The percentage of cells per genotype exceeding this threshold ("Ki67 positive") was calculated.

Transmission electron microscopy and quantitation

Tail, ear, and back skin were harvested from 8-week-old, Krt14$^{C373A/WT}$ and Krt14$^{C373A/null}$, male and female littermates. Back skin was shaved prior to dissection. Harvested tissue was pinned to a wax block and initially fixed for 5 min in ice cold 3% glutaraldehyde/3% paraformaldehyde/ 0.1 M sodium cacodylate (Electron Microscopy Sciences, 15950). Flat, partially fixed tissue was further trimmed into small pieces using fresh razorblades. Subsections were dissected along the sagittal plane of the animal. Tissue pieces were submerged in ice cold 3% glutaraldehyde/3% paraformaldehyde/0.1 M sodium cacodylate and stored at 4 ºC until further processing, which was performed by the Michigan Medicine Microscopy Imaging Laboratory for embedding and sectioning. Tissue pieces were sequentially post-fixed in 1.5% potassium ferrocyanide and 2% osmium tetroxide, extensively washed in buffer and distilled water in-between steps, en-bloc

stained in 2% uranyle acetate, dehydrated in graded series of ethanol (up to 100%) and pure acetone, and embedded in Durcupan epoxy resin using standard procedures. 70-nm thick sections were cut on an ultramicrotome equipped with a diamond knife and imaged using a JEOL JEM 1400 Plus transmission electron microscope. To calculate basal lamina convolution, we traced the basal lamina to measure the distance processed and divided this by the distance covered by a vector connecting the beginning and end of the traced basal lamina.

Analysis of Keratin Phosphorylation by Mass Spectrometry

Pelleted N-TERT keratinocytes were lysed in 6.5 M Urea, 50 mM Tris-HCl pH 7.0, 150 mM sodium chloride, 5 mM ethylenediaminetetraacetic acid (EDTA), 0.1% Triton X-100, 50 μM N-ethylmaleimide supplemented with Protease Inhibitor (A32963, Thermo Fisher Scientific) and Phospho-stop phosphatase inhibitor tablets (A32957, Thermo Fisher Scientific). After ultrasonic homogenizing, the lysate was centrifuged at 15,000xg for 10 minutes at 4°C and the cleared supernatants were loaded onto an SDS-PAGE gel. A gel piece of around 50kDa was cut from the Coomassie-stained gel and proceeded with enzymatic digestion using Trypsin/Lys-C mix (PAV5073, Promega) after reduction with 10 mM Dithiothreitol and alkylation with 50 mM 2-Chloroacetamine (C0267, Sigma-Aldrich). The resulting peptides were extracted and cleaned using C18 and dried in speed-vac. The samples were processed and analyzed at the Mass Spectrometry Facility of the Department of Pathology at the University of Michigan. Around 1 mg of peptides was reconstituted in 5% Formic Acid and analyzed in an Orbitrap Ascend Tribrid mass spectrometer (Thermo Fisher Scientific) equipped with a FAIMS unit. The samples were analyzed in a 60 min gradient using two CVs (-45 and -65V). The full scans (MS1) were acquired over a mass-to-charge (m/z) range of 375-1450 with positive polarity and were allowed for detection in data-dependent acquisition (DDA) mode. For MS1 spectra acquisition, the resolution was set to 120,000, the automatic gain control (AGC) target was 1e6, and the maximum injection time was 251 ms. MS2 spectra acquisition was performed at a resolution of 15,000, with an AGC target of 5e4, a maximum injection time of 27 ms. The isolation window was set to 1.6 m/z, collision energy was set to 25%, dynamic exclusion was 60 seconds, and charge exclusion was unassigned, 1, >6. MS data were processed using Fragpipe v.22.0 [67] against the Homo sapiens UniProt FASTA database (UP000005640). LFQ-phospho workflow was selected. Enzyme specificity was set to trypsin with up to one missed cleavage. The search included cysteine carbamidomethylation as a fixed modification and oxidation of methionine; N-terminal acetylation; serine, threonine and tyrosine phosphorylation as variable modifications. 1% FDR and >0.6 Phosphorylation Localization score was selected.

REFERENCES

1. Blanpain, C., and Fuchs, E. (2009). Epidermal homeostasis: a balancing act of stem cells in the skin. Nature reviews. Molecular cell biology *10*, 207-217. 10.1038/nrm2636.
2. Wells, J.M., and Watt, F.M. (2018). Diverse mechanisms for endogenous regeneration and repair in mammalian organs. Nature *557*, 322-328. 10.1038/s41586-018-0073-7.
3. Fuchs, E. (1995). Keratins and the skin. Ann. Rev. Cell Dev. Biol. *11*, 123-153.
4. Schweizer, J., Bowden, P. E., Coulombe, P. A., Langbein, L., Lane, E. B., Magin, T. M., Maltais, L., Omary, M. B., Parry, D. A., Rogers, M. A., Wright, M. W. (2006). New consensus nomenclature for mammalian keratins. The Journal of cell biology *174*, 169-174. 10.1083/jcb.200603161.
5. Cohen, E., Johnson, C., Redmond, C.J., Nair, R.R., and Coulombe, P.A. (2022). Revisiting the significance of keratin expression in complex epithelia. J Cell Sci *135*. 10.1242/jcs.260594.
6. Li, P., Rietscher, K., Jopp, H., Magin, T.M., and Omary, M.B. (2023). Posttranslational modifications of keratins and their associated proteins as therapeutic targets in keratin diseases. Current opinion in cell biology *85*, 102264. 10.1016/j.ceb.2023.102264.
7. Coulombe, P.A., Kerns, M.L., and Fuchs, E. (2009). Epidermolysis bullosa simplex: a paradigm for disorders of tissue fragility. J Clin Invest *119*, 1784-1793. 38177 [pii] 10.1172/JCI38177.
8. Ramms, L., Fabris, G., Windoffer, R., Schwarz, N., Springer, R., Zhou, C., Lazar, J., Stiefel, S., Hersch, N., Schnakenberg, U., et al. (2013). Keratins as the main component for the mechanical integrity of keratinocytes. Proc Natl Acad Sci U S A *110*, 18513-18518. 10.1073/pnas.1313491110.
9. Lyle, S., Christofidou-Solomidou, M., Liu, Y., Elder, D.E., Albelda, S., and Cotsarelis, G. (1998). The C8/144B monoclonal antibody recognizes cytokeratin 15 and defines the location of human hair follicle stem cells. J Cell Sci *111 (Pt 21)*, 3179-3188. 10.1242/jcs.111.21.3179.
10. Bose, A., Teh, M.T., Mackenzie, I.C., and Waseem, A. (2013). Keratin k15 as a biomarker of epidermal stem cells. Int J Mol Sci *14*, 19385-19398. 10.3390/ijms141019385.
11. Giroux, V., Lento, A.A., Islam, M., Pitarresi, J.R., Kharbanda, A., Hamilton, K.E., Whelan, K.A., Long, A., Rhoades, B., Tang, Q., et al. (2017). Long-lived keratin 15+ esophageal progenitor cells contribute to homeostasis and regeneration. J Clin Invest *127*, 2378-2391. 10.1172/JCI88941.
12. Guo, Y., Redmond, C.J., Leacock, K.A., Brovkina, M.V., Ji, S., Jaskula-Ranga, V., and Coulombe, P.A. (2020). Keratin 14-dependent disulfides regulate epidermal homeostasis and barrier function via 14-3-3σ and YAP1. eLife *9*, e53165. 10.7554/eLife.53165.
13. Lee, C.H., Kim, M.S., Chung, B.M., Leahy, D.J., and Coulombe, P.A. (2012). Structural basis for heteromeric assembly and perinuclear organization of keratin filaments. Nature structural & molecular biology *19*, 707-715. 10.1038/nsmb.2330.
14. Bunick, C.G., and Milstone, L.M. (2017). The X-Ray Crystal Structure of the Keratin 1-Keratin 10 Helix 2B Heterodimer Reveals Molecular Surface Properties and Biochemical Insights into Human Skin Disease. J Invest Dermatol *137*, 142-150. 10.1016/j.jid.2016.08.018.
15. Feng, X., and Coulombe, P.A. (2015). A role for disulfide bonding in keratin intermediate filament organization and dynamics in skin keratinocytes. The Journal of cell biology *209*, 59-72. 10.1083/jcb.201408079.
16. Coulombe, P.A., Kopan, R., and Fuchs, E. (1989). Expression of keratin K14 in the epidermis and hair follicle: insights into complex programs of differentiation. The Journal of cell biology *109*, 2295-2312

17. Totaro, A., Panciera, T., and Piccolo, S. (2018). YAP/TAZ upstream signals and downstream responses. Nat Cell Biol *20*, 888-899. 10.1038/s41556-018-0142-z.
18. Schlegelmilch, K., Mohseni, M., Kirak, O., Pruszak, J., Rodriguez, J.R., Zhou, D., Kreger, B.T., Vasioukhin, V., Avruch, J., Brummelkamp, T.R., and Camargo, F.D. (2011). Yap1 acts downstream of alpha-catenin to control epidermal proliferation. Cell *144*, 782-795. 10.1016/j.cell.2011.02.031.
19. Jonkman, M.F., Heeres, K., Pas, H.H., van Luyn, M.J., Elema, J.D., Corden, L.D., Smith, F.J., McLean, W.H., Ramaekers, F.C., Burton, M., and Scheffer, H. (1996). Effects of keratin 14 ablation on the clinical and cellular phenotype in a kindred with recessive epidermolysis bullosa simplex. J Invest Dermatol *107*, 764-769.
20. Waseem, A., Dogan, B., Tidman, N., Alam, Y., Purkis, P., Jackson, S., Lalli, A., Machesney, M., and Leigh, I.M. (1999). Keratin 15 expression in stratified epithelia: downregulation in activated keratinocytes. J Invest Dermatol *112*, 362-369. 10.1046/j.1523-1747.1999.00535.x.
21. Chan, Y., Anton-Lamprecht, I., Yu, Q.C., Jackel, A., Zabel, B., Ernst, J.P., and Fuchs, E. (1994). A human keratin 14 "knockout": the absence of K14 leads to severe epidermolysis bullosa simplex and a function for an intermediate filament protein. Genes Dev *8*, 2574-2587
22. Rugg, E.L., McLean, I.W.H., Lane, E.B., Pitera, R., McMillan, J.R., Dopping-Hepenstal, P.J.C., Navsaria, H.A., Leigh, I.M., Eady, R.A.J. (1994). A functional "knockout" of human keratin 14. Genes Dev. *8*, 2563-2573.
23. Lloyd, C., Yu, Q.C., Cheng, J., Turksen, K., Degenstein, L., Hutton, E., and Fuchs, E. (1995). The basal keratin network of stratified squamous epithelia: defining K15 function in the absence of K14. The Journal of cell biology *129*, 1329-1344.
24. Fuchs, E., and Green, H. (1980). Changes in keratin gene expression during terminal differentiation of the keratinocyte. Cell *19*, 1033-1042.
25. Stoler, A., Kopan, R., Duvic, M., Fuchs, E. (1988). Use of monospecific antisera and cRNA probes to localize the major changes in keratin expression during normal and abnormal epidermal differentiation. The Journal of cell biology *107*, 427-446.
26. Whitbread, L.A., and Powell, B.C. (1998). Expression of the intermediate filament keratin gene, K15, in the basal cell layers of epithelia and the hair follicle. Experimental cell research *244*, 448-459.
27. Porter, R.M., Lunny, D.P., Ogden, P.H., Morley, S.M., McLean, W.H., Evans, A., Harrison, D.L., Rugg, E.L., and Lane, E.B. (2000). K15 expression implies lateral differentiation within stratified epithelial basal cells. Laboratory investigation *80*, 1701-1710.
28. Webb, A., Li, A., and Kaur, P. (2004). Location and phenotype of human adult keratinocyte stem cells of the skin. Differentiation; research in biological diversity *72*, 387-395. 10.1111/j.1432-0436.2004.07208005.x.
29. Zhan, Q., Signoretti, S., Whitaker-Menezes, D., Friedman, T.M., Korngold, R., and Murphy, G.F. (2007). Cytokeratin15-positive basal epithelial cells targeted in graft-versus-host disease express a constitutive antiapoptotic phenotype. J Invest Dermatol *127*, 106-115. 10.1038/sj.jid.5700583.
30. Cohen, E., Johnson, C.N., Wasikowski, R., Billi, A.C., Tsoi, L.C., Kahlenberg, J.M., Gudjonsson, J.E., and Coulombe, P.A. (2024). Significance of stress keratin expression in normal and diseased epithelia. iScience *27*, 108805. 10.1016/j.isci.2024.108805.
31. Lin, Z., Jin, S., Chen, J., Li, Z., Lin, Z., Tang, L., Nie, Q., and Andersen, B. (2020). Murine interfollicular epidermal differentiation is gradualistic with GRHL3 controlling progression from stem to transition cell states. Nat Commun *11*, 5434. 10.1038/s41467-020-19234-6.
32. Cockburn, K., Annusver, K., Gonzalez, D.G., Ganesan, S., May, D.P., Mesa, K.R., Kawaguchi, K., Kasper, M., and Greco, V. (2022). Gradual differentiation uncoupled from

cell cycle exit generates heterogeneity in the epidermal stem cell layer. Nat Cell Biol *24*, 1692-1700. 10.1038/s41556-022-01021-8.
33. Sambandam, S.A.T., Kasetti, R.B., Xue, L., Dean, D.C., Lu, Q., and Li, Q. (2015). 14-3-3sigma regulates keratinocyte proliferation and differentiation by modulating Yap1 cellular localization. J Invest Dermatol *135*, 1621-1628. 10.1038/jid.2015.42.
34. Sun, B.K., Boxer, L.D., Ransohoff, J.D., Siprashvili, Z., Qu, K., Lopez-Pajares, V., Hollmig, S.T., and Khavari, P.A. (2015). CALML5 is a ZNF750- and TINCR-induced protein that binds stratifin to regulate epidermal differentiation. Genes Dev *29*, 2225-2230. 10.1101/gad.267708.115.
35. Pocaterra, A., Romani, P., and Dupont, S. (2020). YAP/TAZ functions and their regulation at a glance. J Cell Sci *133*. 10.1242/jcs.230425.
36. Pennington, K.L., Chan, T.Y., Torres, M.P., and Andersen, J.L. (2018). The dynamic and stress-adaptive signaling hub of 14-3-3: emerging mechanisms of regulation and context-dependent protein-protein interactions. Oncogene *37*, 5587-5604. 10.1038/s41388-018-0348-3.
37. Kim, S., Wong, P., and Coulombe, P.A. (2006). A keratin cytoskeletal protein regulates protein synthesis and epithelial cell growth. Nature *441*, 362-365. nature04659 [pii] 10.1038/nature04659.
38. Ku, N.O., Liao, J., Omary, M. B. (1998). Phosphorylation of human keratin 18 serine 33 regulates binding to 14-3- 3 proteins. The EMBO journal *17*, 1892-1906.
39. Mariani, R.A., Paranjpe, S., Dobrowolski, R., and Weber, G.F. (2020). 14-3-3 targets keratin intermediate filaments to mechanically sensitive cell-cell contacts. Molecular biology of the cell *31*, 930-943. 10.1091/mbc.E18-06-0373.
40. Tzivion, G., Luo, Z.J., and Avruch, J. (2000). Calyculin A-induced vimentin phosphorylation sequesters 14-3-3 and displaces other 14-3-3 partners in vivo. J Biol Chem *275*, 29772-29778.
41. Madeira, F., Tinti, M., Murugesan, G., Berrett, E., Stafford, M., Toth, R., Cole, C., MacKintosh, C., Barton, G.J. (2015). 14-3-3-Pred: Improved methods to predict 14-3-3-binding phosphopeptides. Bioinformatics *31*, 2276-2283.
42. Liu, Y., Lyle, S., Yang, Z., and Cotsarelis, G. (2003). Keratin 15 promoter targets putative epithelial stem cells in the hair follicle bulge. J Invest Dermatol *121*, 963-968.
43. Trempus, C.S., Morris, R.J., Bortner, C.D., Cotsarelis, G., Faircloth, R.S., Reece, J.M., and Tennant, R.W. (2003). Enrichment for living murine keratinocytes from the hair follicle bulge with the cell surface marker CD34. J Invest Dermatol *120*, 501-511. 10.1046/j.1523-1747.2003.12088.x.
44. Morris, R.J., Liu, Y., Marles, L., Yang, Z., Trempus, C., Li, S., Lin, J.S., Sawicki, J.A., and Cotsarelis, G. (2004). Capturing and profiling adult hair follicle stem cells. Nat Biotechnol *22*, 411-417.
45. Tumbar, T., Guasch, G., Greco, V., Blanpain, C., Lowry, W.E., Rendl, M., and Fuchs, E. (2004). Defining the epithelial stem cell niche in skin. Science *303*, 359-363.
46. Jaks, V., Barker, N., Kasper, M., van Es, J.H., Snippert, H.J., Clevers, H., and Toftgard, R. (2008). Lgr5 marks cycling, yet long-lived, hair follicle stem cells. Nat Genet *40*, 1291-1299. 10.1038/ng.239.
47. Inoue, K., Aoi, N., Sato, T., Yamauchi, Y., Suga, H., Eto, H., Kato, H., Araki, J., and Yoshimura, K. (2009). Differential expression of stem-cell-associated markers in human hair follicle epithelial cells. Lab Invest *89*, 844-856. 10.1038/labinvest.2009.48.
48. Cui, J., Zhao, Q., Song, Z., Chen, Z., Zeng, X., Wang, C., Lin, Z., Wang, F., and Yang, Y. (2022). KLHL24-Mediated Hair Follicle Stem Cells Structural Disruption Causes Alopecia. J Invest Dermatol *142*, 2079-2087 e2078. 10.1016/j.jid.2022.01.007.
49. Wilker, E.W., van Vugt, M.A., Artim, S.A., Huang, P.H., Petersen, C.P., Reinhardt, H.C., Feng, Y., Sharp, P.A., Sonenberg, N., White, F.M., and Yaffe, M.B. (2007). 14-3-3sigma

controls mitotic translation to facilitate cytokinesis. Nature *446*, 329-332. 10.1038/nature05584.
50. Huang, W.G., Cheng, A.L., Chen, Z.C., Peng, F., Zhang, P.F., Li, M.Y., Li, F., Li, J.L., Li, C., Yi, H., et al. (2010). Targeted proteomic analysis of 14-3-3sigma in nasopharyngeal carcinoma. The international journal of biochemistry & cell biology *42*, 137-147. 10.1016/j.biocel.2009.10.001.
51. Reichelt, J., and Magin, T.M. (2002). Hyperproliferation, induction of c-Myc and 14-3-3sigma, but no cell fragility in keratin-10-null mice. J Cell Sci *115*, 2639-2650.
52. Rugg, E.L., McLean, W.H., Lane, E.B., Pitera, R., McMillan, J.R., Dopping-Hepenstal, P.J., Navsaria, H.A., Leigh, I.M., and Eady, R.A. (1994). A functional "knockout" of human keratin 14. Genes & development *8*, 2563-2573.
53. Karczewski, K.J., Francioli, L.C., Tiao, G., Cummings, B.B., Alfoldi, J., Wang, Q., Collins, R.L., Laricchia, K.M., Ganna, A., Birnbaum, D.P., et al. (2020). The mutational constraint spectrum quantified from variation in 141,456 humans. Nature *581*, 434-443. 10.1038/s41586-020-2308-7.
54. Szeverenyi, I., Cassidy, A.J., Chung, C.W., Lee, B.T., Common, J.E., Ogg, S.C., Chen, H., Sim, S.Y., Goh, W.L., Ng, K.W., et al. (2008). The Human Intermediate Filament Database: comprehensive information on a gene family involved in many human diseases. Hum Mutat *29*, 351-360.
55. Coulombe, P.A., and Lee, C.H. (2012). Defining keratin protein function in skin epithelia: epidermolysis bullosa simplex and its aftermath. The Journal of investigative dermatology *132*, 763-775. 10.1038/jid.2011.450.
56. Peters, B., Kirfel, J., Bussow, H., Vidal, M., Magin, T. M. (2001). Complete cytolysis and neonatal lethality in keratin 5 knockout mice reveal its fundamental role in skin integrity and in epidermolysis bullosa simplex. Molecular biology of the cell *12*, 1775-1789.
57. Feng, X., Zhang, H., Margolick, J. B., Coulombe, P. A. (2013). Keratin intracellular concentration revisited: implications for keratin function in surface epithelia. The Journal of investigative dermatology *133*, 850-853. 10.1038/jid.2012.397.
58. Lee, C.H., and Coulombe, P.A. (2009). Self-organization of keratin intermediate filaments into cross-linked networks. The Journal of cell biology *186*, 409-421. jcb.200810196 [pii] 10.1083/jcb.200810196.
59. Ievlev, V., Lynch, T.J., Freischlag, K.W., Gries, C.B., Shah, A., Pai, A.C., Ahlers, B.A., Park, S., Engelhardt, J.F., and Parekh, K.R. (2023). Krt14 and Krt15 differentially regulate regenerative properties and differentiation potential of airway basal cells. JCI Insight *8*. 10.1172/jci.insight.162041.
60. Michel, M., Torok, N., Godbout, M. J., Lussier, M., Gaudreau, P., Royal, A., Germain, L. (1996). Keratin 19 as a biochemical marker of skin stem cells in vivo and in vitro: keratin 19 expressing cells are differentially localized in function of anatomic sites, and their number varies with donor age and culture stage. J Cell Sci *109*, 1017-1028.
61. UniProt, C. (2024). UniProt: the Universal Protein Knowledgebase in 2025. Nucleic acids research. 10.1093/nar/gkae1010.
62. Cheng, J.B., Sedgewick, A.J., Finnegan, A.I., Harirchian, P., Lee, J., Kwon, S., Fassett, M.S., Golovato, J., Gray, M., Ghadially, R., et al. (2018). Transcriptional Programming of Normal and Inflamed Human Epidermis at Single-Cell Resolution. Cell reports *25*, 871-883. 10.1016/j.celrep.2018.09.006.
63. Leyva-Castillo, J.M., Sun, L., Wu, S.Y., Rockowitz, S., Sliz, P., and Geha, R.S. (2022). Single-cell transcriptome profile of mouse skin undergoing antigen-driven allergic inflammation recapitulates findings in atopic dermatitis skin lesions. J Allergy Clin Immunol *150*, 373-384. 10.1016/j.jaci.2022.03.002.

64. Germain, P.L., Lun, A., Garcia Meixide, C., Macnair, W., and Robinson, M.D. (2021). Doublet identification in single-cell sequencing data using scDblFinder. F1000Res *10*, 979. 10.12688/f1000research.73600.2.
65. Kuleshov, M.V., Jones, M.R., Rouillard, A.D., Fernandez, N.F., Duan, Q., Wang, Z., Koplev, S., Jenkins, S.L., Jagodnik, K.M., Lachmann, A., et al. (2016). Enrichr: a comprehensive gene set enrichment analysis web server 2016 update. Nucleic acids research *44*, W90-97. 10.1093/nar/gkw377.
66. Franzen, O., Gan, L.M., and Bjorkegren, J.L.M. (2019). PanglaoDB: a web server for exploration of mouse and human single-cell RNA sequencing data. Database (Oxford) *2019*. 10.1093/database/baz046.
67. Kong, A.T., Leprevost, F.V., Avtonomov, D.M., Mellacheruvu, D., and Nesvizhskii, A.I. (2017). MSFragger: ultrafast and comprehensive peptide identification in mass spectrometry-based proteomics. Nature methods *14*, 513-520. 10.1038/nmeth.4256.

FIGURES LEGENDS

Figure 1. K14 and K15 display distinct staining patterns in vivo and ex vivo. A. Individual immunostaining for keratin 14 (K14) and keratin 15 (K15) in formalin-fixed, paraffin embedded human buttocks skin. Dashed line specifies the basal lamina. epi, epidermis; derm, dermis. Scale bar, 50 µm. **B.** Multiplexed immunostaining for keratin 15 (K15, green) and keratin 10 (K10, red). Nuclei are counterstained with DAPI (blue). Dashed line specifies the basal lamina. Scale bar = 50 µm. **B'.** Subset of boxed region in Fig. 1B. Grayscale single channels for K15 and K10 and merged multiplex (K15 = green, K10 = red, DAPI = blue). Dashed line specifies the basal lamina. Scale bar, 50 µm. Arrow indicates a K15-positive, K15-negative basally-located keratinocyte. **C.** Individual immunostaining for keratin 14 (K14) and keratin 15 (K15) in skin keratinocytes harvested from neonatal *Krt14*$^{C373A/WT}$ pups and seeded in primary culture. Scale bar, 50 µm. **C'.** Scatter plots representing the K14 and K15 mean intensity values of individually traced cells in Fig. 1C (mean ± SD).

Figure 2: Relationships between *KRT14, KRT15 and KRT10* in human trunk skin. **A,B.** UMAP of human trunk epidermis highlighting *KRT15* levels (green) and (A) *KRT14* or (B) *KRT10* levels (red) across Seurat clusters. **C.** Single cell expression of *KRT15* mapped against *KRT14* levels in 26,063 keratinocytes in the human trunk epidermis dataset. **D.** Distribution of *KRT14* and *KRT15* expression across all keratinocytes in dataset. **E.** Distribution of *KRT15, KRT14* and *KRT10* expression in cells exhibiting increasing levels of 'Basal Score' signature genes (see "Methods" for definition of composite scores). **F.** Analysis of average keratin expression level across 17 Seurat clusters matching keratinocyte signatures in the human trunk epidermis dataset. *KRT14* (red, circle), *KRT15* (green, square) and *KRT10* (blue, triangle) assessed per cluster. Clusters are sorted on the X axis according to the highest basal score to differentiation score ratio. The Seurat cluster showing the highest G2M composite score, on average, is highlighted. (G) Expression of G2M composite score relative to *KRT14* and *KRT15* levels across keratinocytes in human trunk epidermis. (H) Comparison of linear pairwise expression of type I and type II keratins *KRT14/KRT5* (red, R^2=0.79), *KRT10/KRT1* (blue, R^2=0.84), and *KRT15/KRT5* (green, R^2=0.31) across all keratinocytes in the human trunk epidermis dataset. (H') Heatmap summarizing Pearson (r) correlations between type I and type II keratins across the dataset.

Figure 3. *KRT15* and *KRT10* expression define the extremities of the basal keratinocyte differentiation spectrum. A. Top 24 correlated genes for *KRT15* and *KRT10* in trunk skin keratinocytes. **B.** Bar graph showing all GO categories enriched for *KRT15*-correlated genes with a cutoff of $P < 0.05$ from GProfiler. **C.** Bar graph showing all GO categories enriched for *KRT10*-correlated genes with a cutoff of $P < 0.05$ from GProfiler.

Figure 4. The stutter cysteine is sufficient to relocalize YAP1 in transfected HeLa cells. **A.** Diagram of K14 and K15 primary structures. Boxes represent coiled-coil regions. Schematic comparing the orthologous residues between K14 and K15 in the putative regulatory regions in the head and 2B rod domains. Mouse K14 contains 4 cysteines in the head domain and 2 in the 2B rod domain. Mouse K15 contains 1 cysteine residue in the head domain and 2 in the 2B rod domain. K15 does not have a cysteine orthologous to mK14 C373 (mK15 C373 is downstream

of the mK15 stutter region). **B.** Representative images of HeLa cells transfected with mCherry-K5, EGFP-K14, and untagged WT and mutant K15. mCherry signal is autofluorescence, YAP1 is visualized through immunostaining. Arrowheads depict cells with strong nuclear YAP1 staining. Scale bar, 10 μm. **C.** Scatter plots representing 3 pooled independent replicates, displaying mean and standard deviation. Dots represent a single cell. Comparisons made using Mann-Whitney tests. **** P <0.0001, *** P = 0.0002 and 0.0003, ** P = 0.0083.

Figure 5. The stutter cysteine is sufficient to relocalize YAP1 in response to keratinocyte differentiation. A. Representative micrographs of *Krt14*$^{WT/null}$ keratinocytes in primary culture transfected with EGFP-K14, EGFP-K15, or EGFP-K15 A351C, with and without 1.2 mM $CaCl_2$ to induce differentiation. YAP1 is visualized through immunofluorescence. "Merge" panels display autofluorescent EGFP (green) and YAP1 (magenta). Arrowheads indicate EGFP-positive keratinocytes. Scale bar, 10 μm. **B.** Scatter plots representing 3 independent replicates, pooled, displaying mean ± SD. Dots represent a single cell. Comparisons made using unpaired t tests with Welch's correction. **** P <0.0001, ** P = 0.0058 and 0.0014. **C.** Multiplexed immuno-staining for K15 (green) and YAP1 (red). Nuclei are counterstained with DAPI (blue). Dashed line specifies the basal lamina. epi, epidermis; derm, dermis. Scale bar, 50 μm. Arrowheads depict region with strong K15 and nuclear YAP1 staining. XY scatter plot is comparing nuclear YAP1 intensity (arbitrary units) vs. K15 intensity (arbitrary units). Each dot represents a single basal keratinocyte. Equation for the simple linear regression of the comparison is displayed, showing a positive correlation. This regression is significantly nonzero (P <0.0001).

Figure 6. The SCRAPS motif and the stutter cysteine are required to interconvert YAP1-interaction of K14 and K15. A. Representative micrographs of YAP1-14-3-3σ proximity ligation assay performed on transfected HeLa cells. Cells were transfected with untagged keratin 5 and WT and mutant K14 or K15. Merge panels show PLA punctae (red), EGFP-tagged keratin autofluorescence (green), and DAPI counterstain (blue). Scale bar = 10 μm. **B.** Scatter plots representing YAP1-14-3-3σ PLA punctae counted per cell in 3 pooled independent replicates, displaying mean and standard deviation. Dots represent a single cell. Comparisons made using Mann-Whitney tests. **** P <0.0001, ** P = 0.0033, ns = not significant.

Figure 7. K15 overrepresentation alters keratinocyte homeostasis *in vivo*. A. *Krt14*$^{C373A/WT}$ and *Krt14*$^{C373A/null}$ (arrow) littermates at P5. **B.** H&E staining performed on back skin harvested from P5 *Krt14*$^{C373A/WT}$ and *Krt14*$^{C373A/null}$ littermate pups. Scale bar, 50 μm. **C.** H&E staining performed on tail tissue harvested from 8 week old *Krt14*$^{C373A/WT}$ and *Krt14*$^{C373A/null}$ tail tissue. Scale bar = 50 μm. **D.** Mean cytoplasmic area of basal keratinocytes with standard deviation. Dots represent single cells. Comparisons made using Mann-Whitney tests. * P = 0.0286. **E.** Basal cell density calculated by mean cells/μm of basal lamina with standard deviation. Dots represent individual micrographs from tail skin harvested from 4 littermate animals each. Comparisons made using Mann-Whitney tests. * P = 0.014. **F.** Ki67 immunofluorescence performed on 8 week old *Krt14*$^{C373A/WT}$ and *Krt14*$^{C373A/null}$ littermate tail skin. Merge panel displays Ki67 (green) with DAPI counterstain (red). Arrows indicate Ki67-positive basal nuclei. Dashed line specifies the basal lamina. epi, epidermis; derm, dermis. Scale bar, 50 μm. **G.** Mean of the Ki67 mean intensity value for individual basal keratinocyte nuclei, displayed with standard deviation. Percentages of cells above the visual threshold for Ki67 positivity (green dashed line).

Comparisons made using Mann-Whitney tests. **** P <0.0001.**H.** Representative transmission electron microscopy micrographs of basal keratinocytes in ear skin if 8 week old *Krt14*$^{C373A/WT}$ and *Krt14*$^{C373A/null}$. Nu, nucleus; kf, keratin filaments; arrows, hemidesmosomes; *, areas devoid of keratin filaments. Scale bar, 800 nm. **I.** Mean of the basal lamina processed/ distance covered to represent basal lamina convolution, displayed with standard deviation. Dots are individual micrograph images. Comparisons made using Mann-Whitney tests. *** P = 0.0009.

Figure 8. Modeling the interplay of keratin 15 and keratin 14 in regulating YAP1's access to the nucleus is progenitor keratinocytes of the epidermis. The model proposes that a higher K15:K14 protein ratio in basal keratinocytes of epidermis promotes the progenitor state and antagonizes differentiation. See text for details.

Figure 1. Redmond et al.

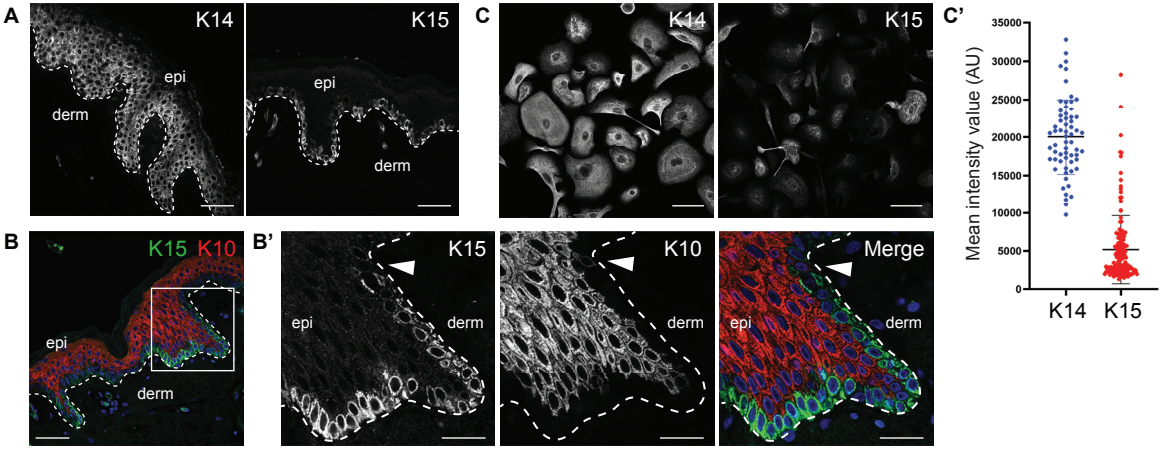

Figure 2 - Redmond et al.

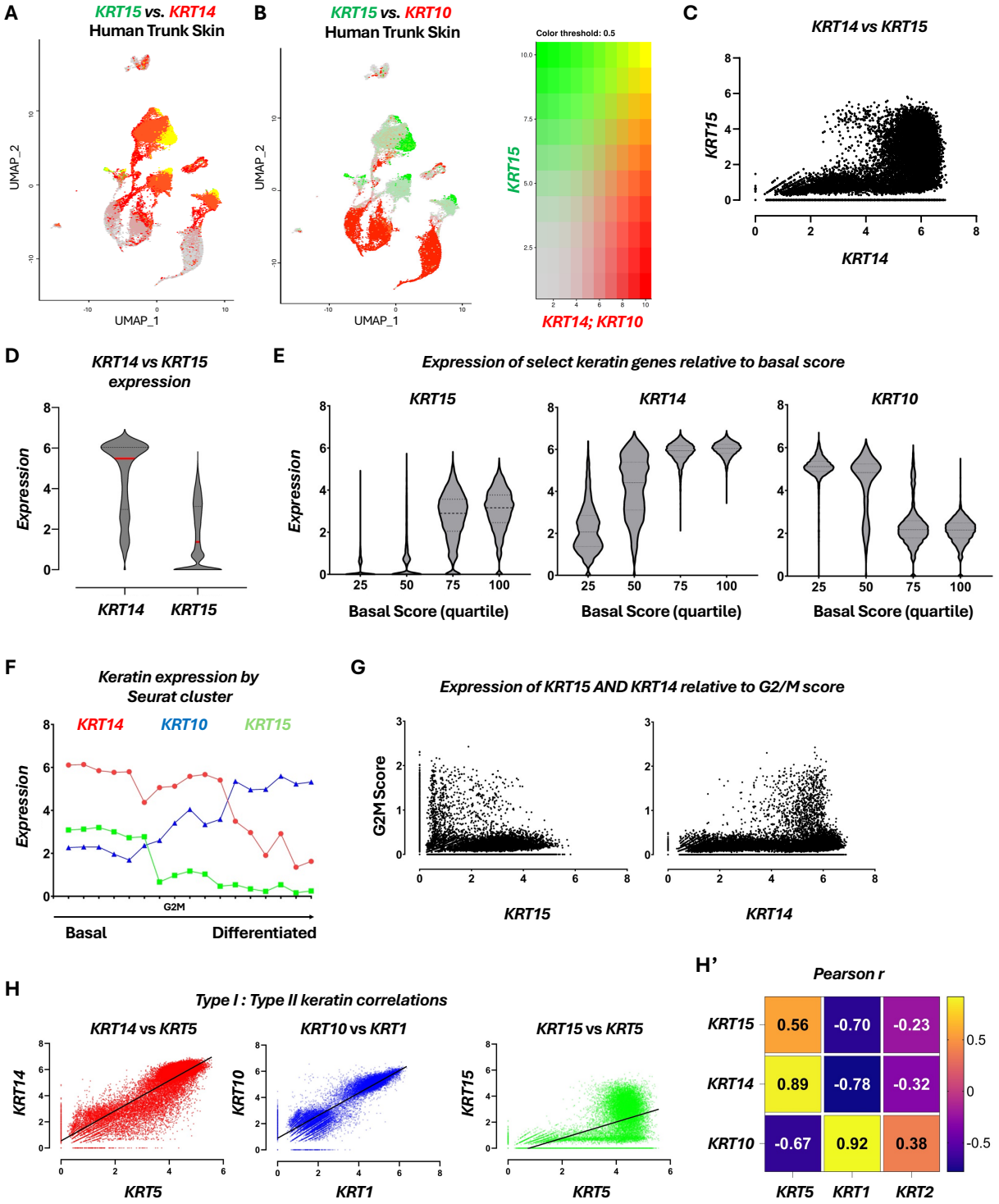

Figure 3. Redmond et al.

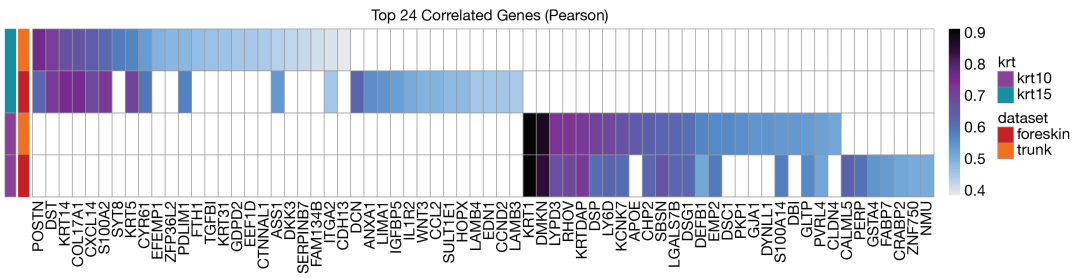

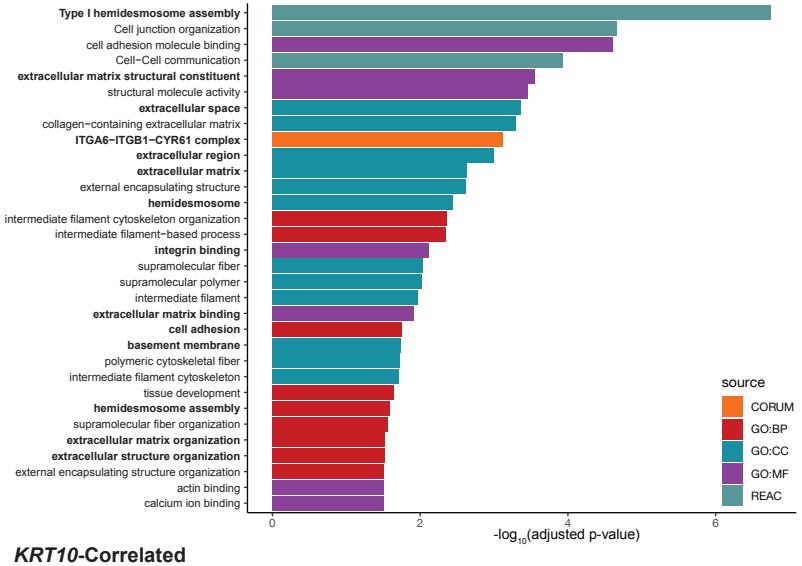

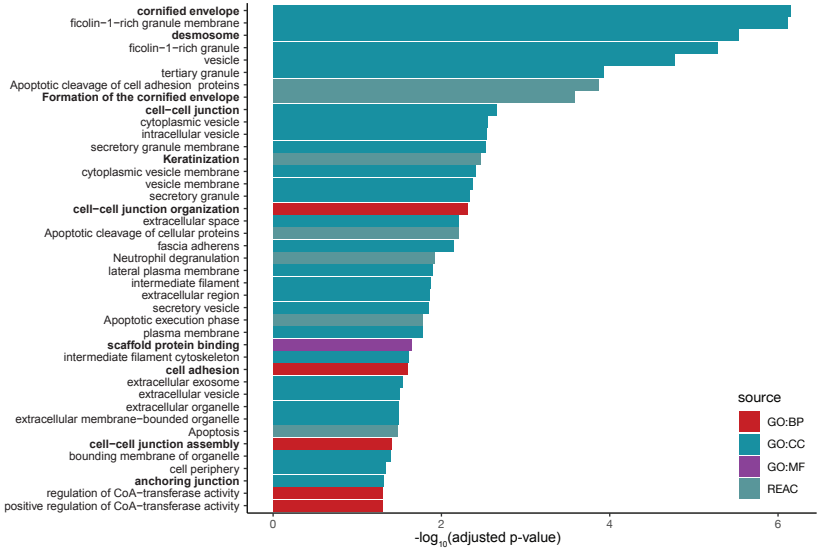

Figure 4 - Redmond et al.

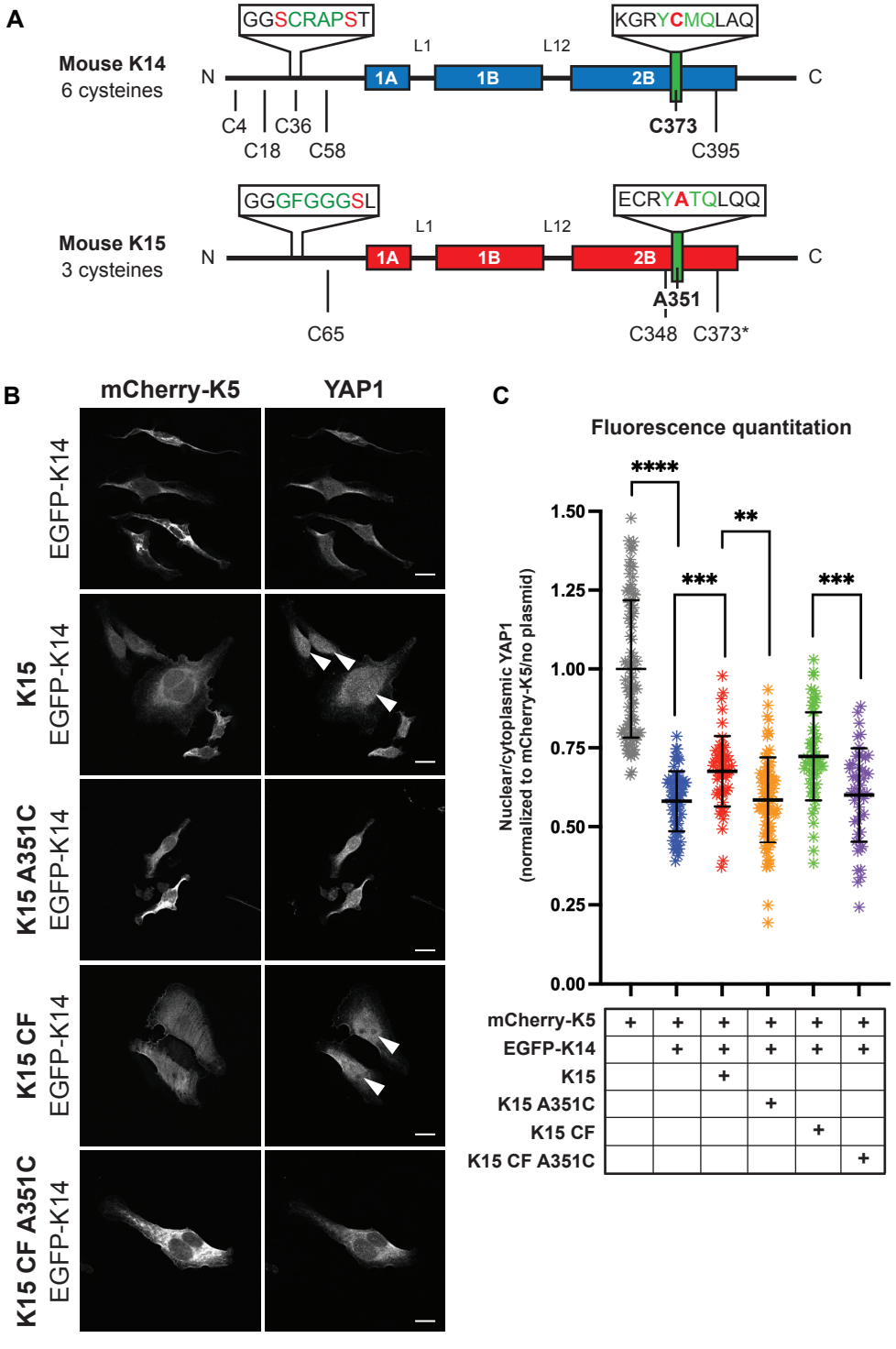

Figure 5 - Redmond et al.

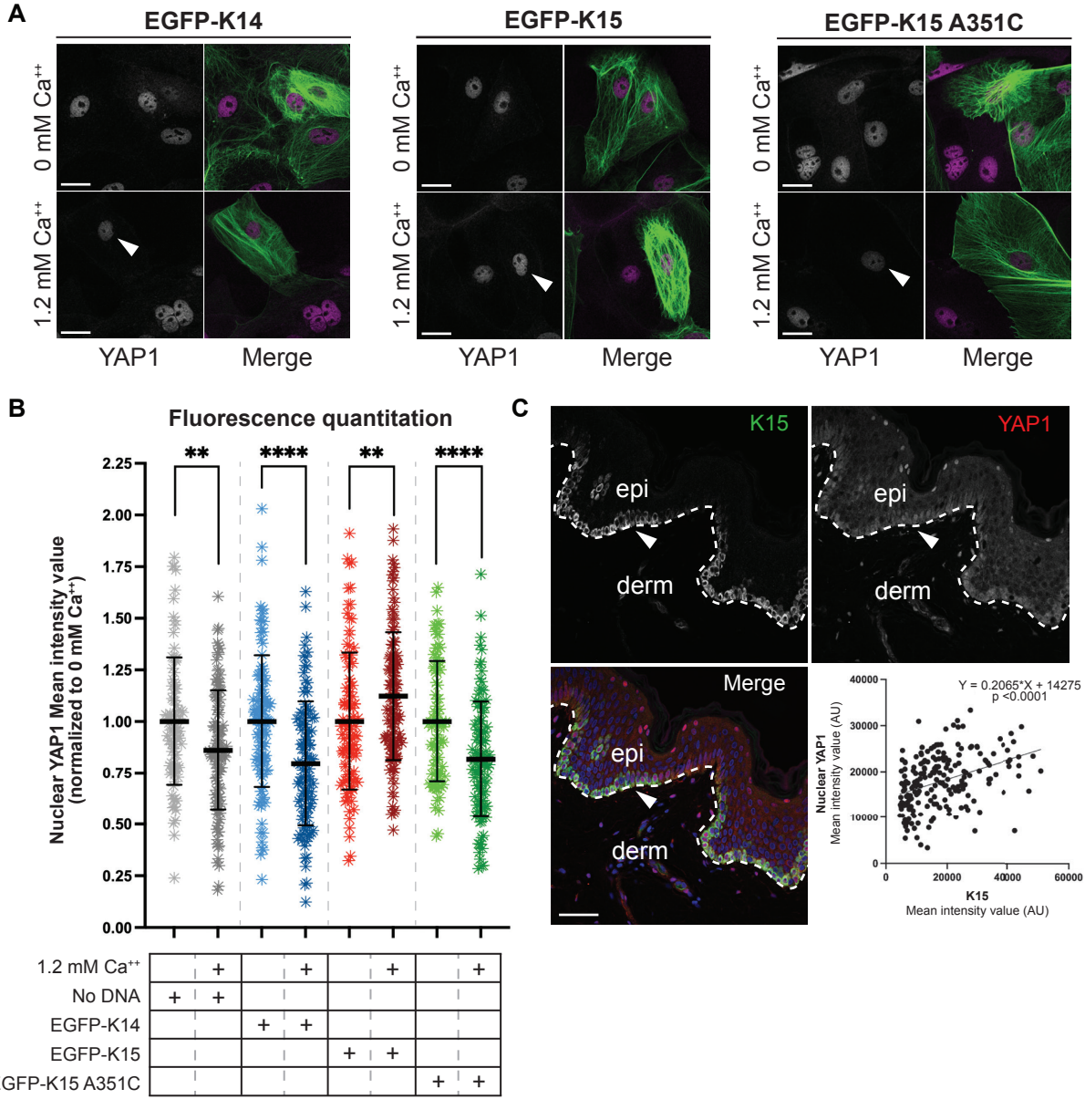

Figure 6 - Redmond et al.

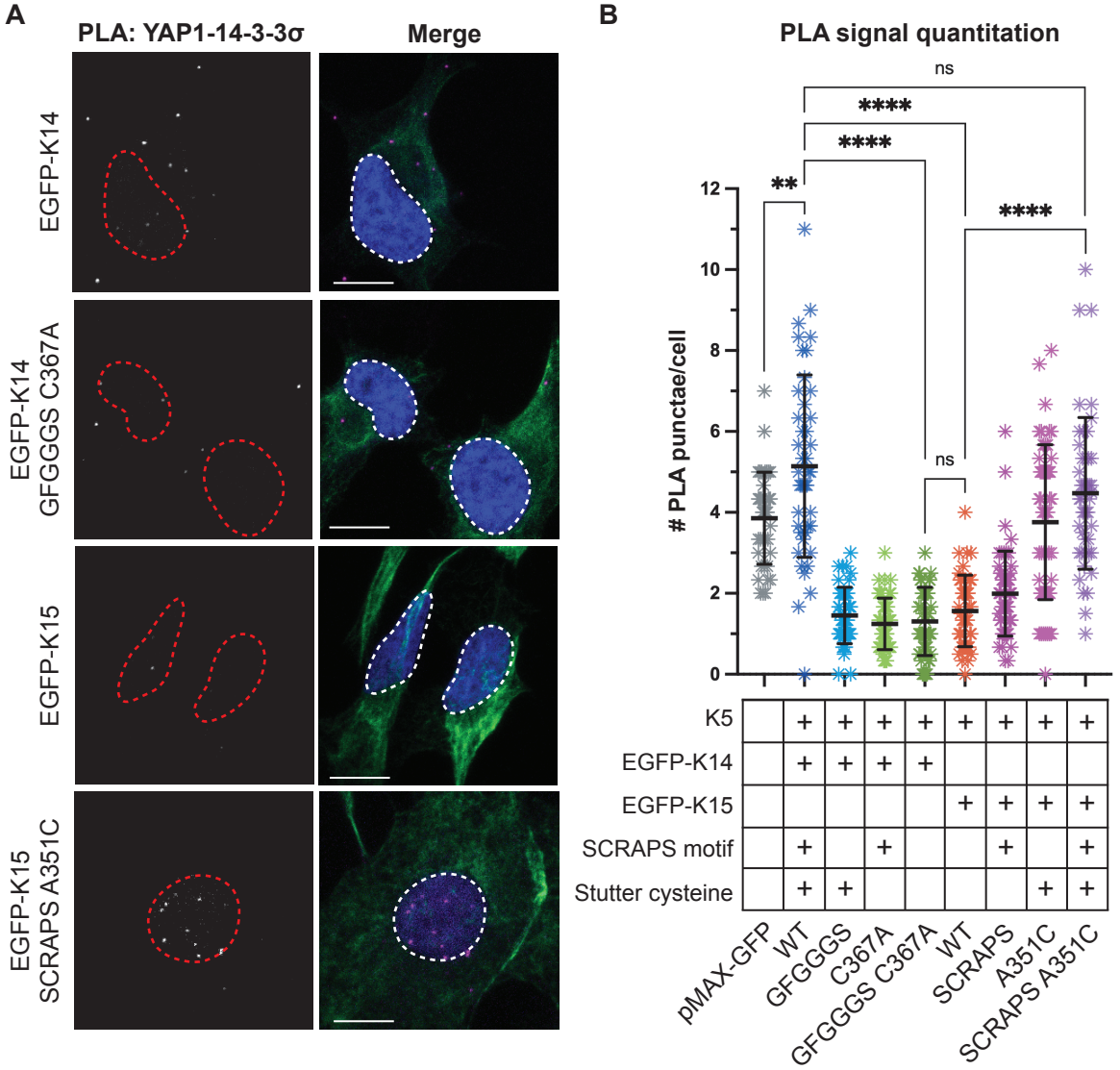

Figure 7. Redmond et al.

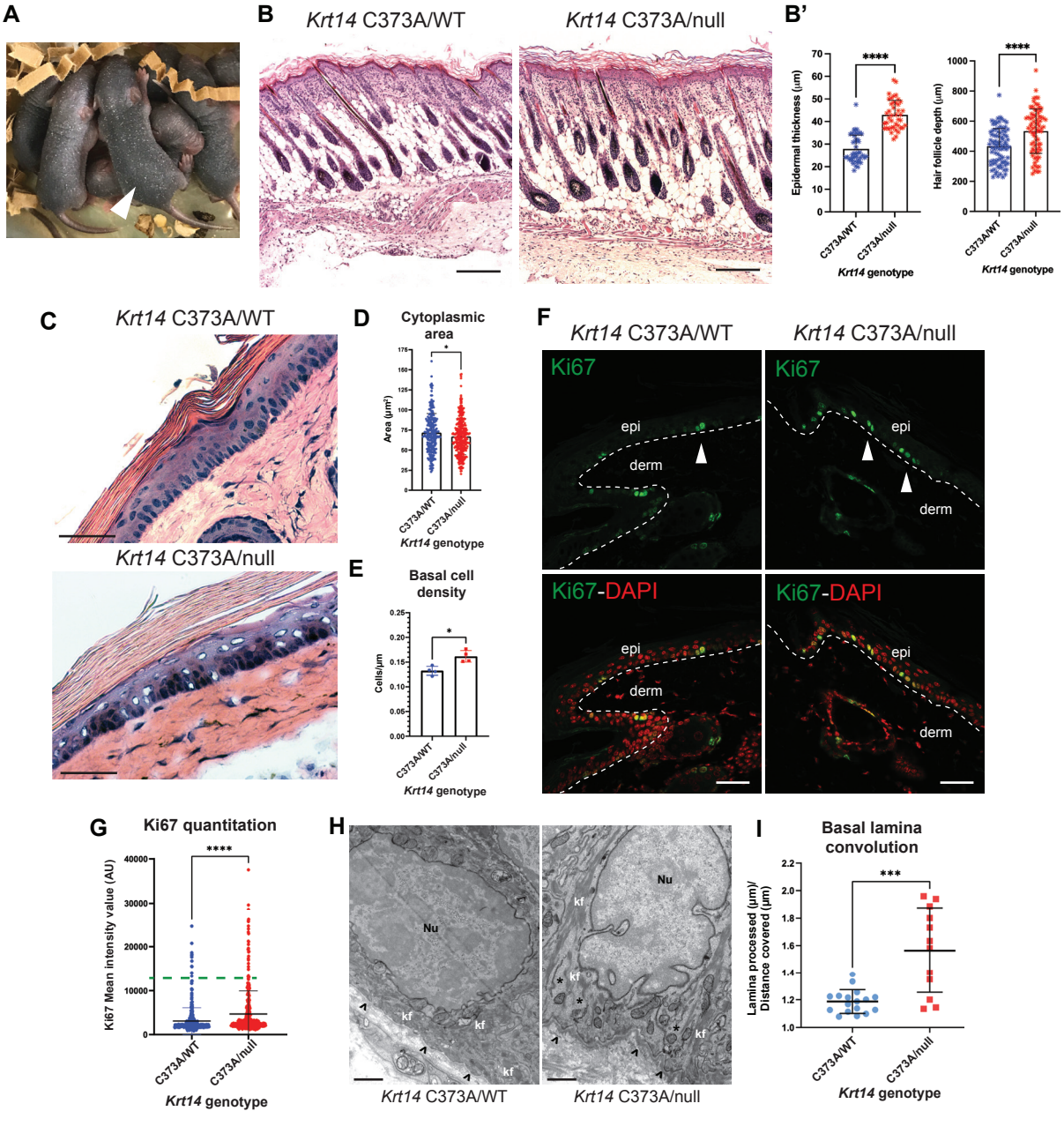
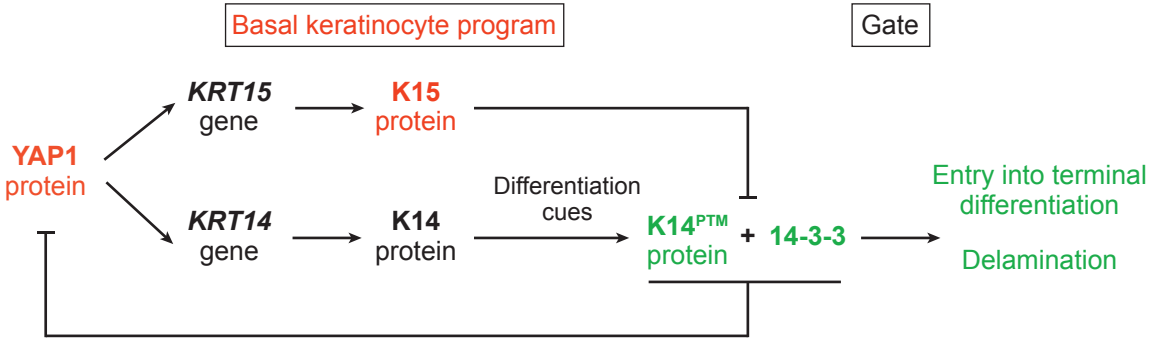
Figure 8. Redmond et al.